

# Sampling Theory for Function Approximation with Numerical Redundancy

Astrid Herremans\* and Daan Huybrechs\*

## Abstract

We explore the interaction between numerical rounding errors and discretization errors involved in linear function approximation schemes. To precisely identify when numerical effects become significant, we introduce the concept of *numerical redundancy*: a set of functions is numerically redundant if, due to finite-precision arithmetic, it spans a lower-dimensional space numerically than it does analytically. This phenomenon arises in a variety of settings, though it is not always explicitly identified as such. When such a set is used as a basis for numerical approximations, recovering the expansion coefficients of the best approximation is generally impossible. More specifically, we show that approximations produced by practical algorithms—affected by rounding errors—are implicitly subject to  $\ell^2$ -regularization. The computed solutions, therefore, exhibit reduced accuracy compared to the best approximation. On the other hand, there is also a benefit: regularization reduces the amount of data needed for accurate and stable discrete approximation. The primary aim of this paper is to develop the tools needed to fully understand this effect. Additionally, we present a constructive method for optimally selecting random data points for  $L^2$ -approximations, explicitly accounting for the influence of rounding errors. We illustrate our results in two typical scenarios that lead to numerical redundancy: (1) approximation on irregular domains and (2) approximation that incorporate specific features of the function to be approximated. In doing so, we obtain new results on random sampling for Fourier extension frames.

**Keywords.** function approximation, weighted least squares, regularization, orthogonalization, frames theory

**MSC codes.** 42C15, 41A65, 65F22, 65T40, 65F25

## 1 Introduction

We consider the problem of computing an approximation to a function  $f$  in a Hilbert space  $H$ . Due to the focus on computability, this problem will be referred to as numerical approximation. An important aspect is that although the function  $f$  generally resides in an infinite-dimensional space, a numerical method can process only a finite number of measurements of  $f$ . This naturally leads to the introduction of a sequence of finite-dimensional spaces  $\{V_n\}_{n \in \mathbb{N}}$  of increasing dimension  $n$ , forming approximations to  $H$ . It is hereby assumed, based on prior knowledge, that  $f$  is well approximated in the spaces  $V_n$  in the sense that fast convergence is attainable. Associated with a numerical approximation is thus an operator  $\mathcal{F}_{n,m} : \mathbb{C}^m \rightarrow V_n$  mapping  $m$  measurements of a function  $f$  to a function  $f_{n,m}$  in the approximation space  $V_n$ . Note that the number of measurements  $m$  can differ from the dimension  $n$ . In particular, it is often required that  $m$  is sufficiently large compared to  $n$ , or equivalently  $n$  sufficiently small, in order to obtain robust and accurate approximation methods [4, 20].

Another important aspect of numerical approximation is how to represent an approximation in  $V_n$ . To this end, one chooses a spanning set  $\Phi_n = \{\phi_{i,n}\}_{i=1}^{n'}$  satisfying  $\text{span}(\Phi_n) = V_n$ . This allows the approximation  $f_{n,m}$  to be characterized by a set of expansion coefficients  $\mathbf{x}$

$$f_{n,m} = \sum_{i=1}^{n'} x_i \phi_{i,n}. \quad (1)$$

---

\*Department of Computer Science, KU Leuven, 3001 Leuven, Belgium (astrid.herremans@kuleuven.be, daan.huybrechs@kuleuven.be)

Note that the spanning set  $\Phi_n$  does not need to be linearly independent, implying that  $n'$  can differ from  $n$ , in which case multiple sets of expansion coefficients exist that describe the same function. Associated with a numerical approximation is, therefore, also an operator  $\mathcal{L}_{n,m} : \mathbb{C}^m \rightarrow \mathbb{C}^{n'}$  mapping  $m$  measurements of a function  $f$  to a set of  $n'$  expansion coefficients of an approximation  $f_{n,m} \in V_n$ .

In sampling theory, the central goal is to determine how much information about  $f$  is needed to construct a (near-)optimal approximation in  $V_n$ , while ensuring robustness to noise. Classical results for linear approximation are typically obtained by analysing  $\mathcal{F}_{n,m}$ , and are thus independent of the choice of the spanning set  $\Phi_n$  for  $V_n$ . The underlying assumption is that the numerical computations are performed using an orthonormal or Riesz basis, such that  $\mathcal{L}_{n,m}$  and  $\mathcal{F}_{n,m}$  have similar properties.

However, this assumption is often violated. In particular, computational methods frequently use numerically redundant spanning sets  $\Phi_n$ —that is, due to finite-precision arithmetic, the functions in  $\Phi_n$  span a lower-dimensional space numerically than they do in exact arithmetic. This leads to discretized systems that are numerically rank-deficient, and hence subject to significant rounding errors. In order to understand what happens numerically, the analysis must account for the interaction between rounding and discretization errors. Unlike in classical settings, it is no longer sufficient to only study  $\mathcal{F}_{n,m}$ ; the analysis heavily depends on  $\mathcal{L}_{n,m}$  making our results inherently dependent on the choice of representation  $\Phi_n$ , not merely on the approximation space  $V_n$ .

Numerical redundancy arises in a number of settings. For example, in function approximation on irregular domains, orthonormal or Riesz bases are not readily available. A standard strategy in such settings is to restrict a known basis—originally defined on a surrounding, regular domain—to the target approximation domain, yielding a numerically redundant spanning set [40]. Note that the target domain may sometimes be unknown, as is often the case for high-dimensional approximation methods arising in uncertainty quantification [7]. Redundancy also occurs when bases are combined, enriched or weighted to better capture specific features of the function being approximated [31, 45, 33]. Other settings of numerical redundancy include radial basis function approximations [46], Trefftz methods [37], and deep neural networks [3]. The analysis of redundant sets for numerical approximation was initiated in [6, 8].

In the presence of numerical redundancy, the coefficients corresponding to the best approximation are generally not computable. Instead, practical algorithms affected by rounding errors compute approximations that are effectively  $\ell^2$ -regularized. While some numerical methods attempt to circumvent this by orthogonalizing the basis, we demonstrate that standard numerical orthogonalization techniques are not able to mitigate the effects of finite-precision arithmetic. Therefore, our results apply broadly across many numerical approximation schemes that rely on redundant representations.

We describe the approximation problem in more detail and give known results about sampling for least squares approximations before stating the main contribution and overview of the paper.

## 1.1 Approximation problem

Let  $f$  be a function in a separable Hilbert space  $H$  with associated inner product  $\langle \cdot, \cdot \rangle_H$  and induced norm  $\| \cdot \|_H$ . We aim at computing approximations to  $f$  in a sequence of finite-dimensional approximation spaces  $\{V_n\}_{n \in \mathbb{N}}$  of increasing dimension  $n$ , satisfying  $V_n \subset H$ . We assume that we can process measurements  $\mathcal{M}_m f$  ( $m = 1, 2, \dots$ ), where  $\mathcal{M}_m$  are linear sampling operators

$$\mathcal{M}_m : G \rightarrow \mathbb{C}^m, \quad f \mapsto \{l_{j,m}(f)\}_{j=1}^m \quad (2)$$

consisting of  $m$  functionals  $l_{j,m}$ , which may depend on  $m$ . The operators  $\mathcal{M}_m$  may only be defined on a dense subspace  $G \subseteq H$  with associated norm  $\| \cdot \|_G$ , satisfying

$$\|g\|_H^2 \leq C_G \|g\|_G^2, \quad \forall g \in G. \quad (3)$$

We assume that each  $\mathcal{M}_m$  is bounded with respect to  $\| \cdot \|_G$ , i.e.,

$$\|\mathcal{M}_m\|_{G,2} := \sup_{g \in G, g \neq 0} \frac{\|\mathcal{M}_m g\|_2}{\|g\|_G} < \infty,$$

and that  $V_n \subset G$  for all  $n \in \mathbb{N}$ . In what follows, we will also assume that  $\|\mathcal{M}_m\|_{G,2} \geq 1$ , which can always be achieved via scaling. The operator  $\mathcal{M}_m$  defines a semi-norm

$$\| \cdot \|_m := \|\mathcal{M}_m \cdot \|_2. \quad (4)$$

**Remark 1.** A typical example is the approximation of continuous functions in  $H = L^2([-1, 1])$  using pointwise evaluations. In this case,  $G$  can be the space of continuous functions  $C([-1, 1])$  with associated norm  $\|g\|_G = \sup_{x \in [-1, 1]} |g(x)|$  satisfying (3) for  $C_G = 2$ . Furthermore, if

$$\mathcal{M}_m f = \{f(x_{j,m})/\sqrt{m}\}_{j=1}^m$$

for some sample points  $x_{j,m} \in [-1, 1]$ , then  $\|\mathcal{M}_m\|_{G,2} = 1$ .

In order to represent the approximations, we use spanning sets  $\Phi_n = \{\phi_{i,n}\}_{i=1}^{n'}$  which satisfy  $\text{span}(\Phi_n) = V_n$  for all  $n \in \mathbb{N}$ . The elements  $\phi_{i,n}$  may depend on  $n$  and characterize the synthesis operator

$$\mathcal{T}_n : \mathbb{C}^{n'} \rightarrow V_n, \quad \mathbf{x} \mapsto \sum_{i=1}^{n'} x_i \phi_{i,n}. \quad (5)$$

Note that  $n'$  depends on  $n$  yet it is not necessarily equal to  $n$ , since  $\Phi_n$  can in general be linearly dependent. For a certain operator  $\mathcal{L}_{n,m} : \mathbb{C}^m \rightarrow \mathbb{C}^{n'}$  from measurements to expansion coefficients, one can now define the approximation  $f_{n,m} \in V_n$  as

$$f_{n,m} := \mathcal{T}_n \mathcal{L}_{n,m} (\mathcal{M}_m f + \mathbf{n}) = \mathcal{F}_{n,m} (\mathcal{M}_m f + \mathbf{n}), \quad (6)$$

where

$$\mathcal{F}_{n,m} : \mathbb{C}^m \rightarrow V_n, \quad \mathbf{d} \mapsto \mathcal{T}_n \mathcal{L}_{n,m} \mathbf{d} \quad (7)$$

and  $\mathbf{n} \in \mathbb{C}^m$  is measurement noise. The question arises whether the approximation is accurate, i.e., whether it lies close to the best approximation in  $V_n$  and is robust to measurement noise. We will first discuss the well-studied case of least squares approximation.

## 1.2 Least squares approximation

A typical choice for the map  $\mathcal{L}_{n,m}$  is discrete least squares fitting,

$$\mathcal{L}_{n,m}^{\text{LS}} : \mathbb{C}^m \rightarrow \mathbb{C}^{n'}, \quad \mathbf{d} \mapsto \arg \min_{\mathbf{x} \in \mathbb{C}^{n'}} \|\mathcal{M}_m \mathcal{T}_n \mathbf{x} - \mathbf{d}\|_2^2 \quad (8)$$

with associated operator  $\mathcal{F}_{n,m}^{\text{LS}}$  defined by (7). The least squares operator  $\mathcal{L}_{n,m}^{\text{LS}}$  is linear. For simplicity, we assume that the operator is also uniquely defined, implying that  $m \geq n = n'$ . The accuracy of a least squares approximation has been studied extensively, see for example [2, 5, 14, 20]. A key ingredient to its analysis is the norm inequality

$$A_{n,m} \|v\|_H^2 \leq \|v\|_m^2, \quad \forall v \in V_n. \quad (9)$$

Similar to [2, Theorem 5.3], the following theorem shows that if the sampling operator satisfies (9) for some  $A_{n,m} > 0$ , then the error of the discrete least squares approximation is close to optimal and the influence of measurement noise is bounded.

**Theorem 1.** If (9) holds for some  $A_{n,m} > 0$ , then the error of the discrete least squares approximation to  $f \in H$  satisfies

$$\|f - \mathcal{F}_{n,m}^{\text{LS}} \mathbf{f}\|_H \leq \left( \sqrt{C_G} + \frac{\|\mathcal{M}_m\|_{G,2}}{\sqrt{A_{n,m}}} \right) e_n(f) + \frac{1}{\sqrt{A_{n,m}}} \|\mathbf{n}\|_2,$$

where  $\mathbf{f} = \mathcal{M}_m f + \mathbf{n} \in \mathbb{C}^m$  is noisy data and

$$e_n(f) := \inf_{v \in V_n} \|f - v\|_G. \quad (10)$$

*Proof.* If  $f \notin G$ , then the right-hand side is infinite such that the bound trivially holds. Assuming  $f \in G$ , one has for any  $v \in V_n$

$$\begin{aligned}
\|f - \mathcal{F}_{n,m}^{\text{LS}} \mathbf{f}\|_H &\leq \|f - v\|_H + \|v - \mathcal{F}_{n,m}^{\text{LS}} \mathbf{f}\|_H \\
&\leq \|f - v\|_H + \frac{1}{\sqrt{A_{n,m}}} \|v - \mathcal{F}_{n,m}^{\text{LS}} \mathbf{f}\|_m && \text{(using (9))} \\
&\leq \|f - v\|_H + \frac{1}{\sqrt{A_{n,m}}} \|\mathcal{M}_m v - \mathbf{f}\|_2 \\
&\leq \|f - v\|_H + \frac{1}{\sqrt{A_{n,m}}} (\|v - f\|_m + \|\mathbf{n}\|_2) \\
&\leq \left( \sqrt{C_G} + \frac{\|\mathcal{M}_m\|_{G,2}}{\sqrt{A_{n,m}}} \right) \|f - v\|_G + \frac{1}{\sqrt{A_{n,m}}} \|\mathbf{n}\|_2 && \text{(boundedness of } \mathcal{M}_m \text{ and (3))}
\end{aligned}$$

where in the third step we used that  $\mathcal{M}_m \mathcal{F}_{n,m}^{\text{LS}}$  is a projection onto  $\{\mathcal{M}_m v \mid v \in V_n\}$  such that

$$\|\mathcal{M}_m v - \mathcal{M}_m \mathcal{F}_{n,m}^{\text{LS}} \mathbf{f}\|_2 = \|\mathcal{M}_m \mathcal{F}_{n,m}^{\text{LS}} \mathcal{M}_m v - \mathcal{M}_m \mathcal{F}_{n,m}^{\text{LS}} \mathbf{f}\|_2 \leq \|\mathcal{M}_m v - \mathbf{f}\|_2.$$

□

**Remark 2.** *In this paper, we limit ourselves to error bounds that depend on the optimal error measured in the  $G$ -norm. Deriving bounds in terms of the  $H$ -norm typically requires additional effort. For instance, probabilistic error bounds of this kind can be obtained when considering random pointwise samples for  $H = L^2$  approximations, as demonstrated in [21, 25].*

**Remark 3.** *Assume that we can identify a function  $\gamma : \mathbb{N} \rightarrow \mathbb{N}$  such that there exists a constant  $A$  satisfying  $0 < A \leq A_{n,\gamma(n)}$  for all  $n \in \mathbb{N}$ . Then, the operators  $\mathcal{F}_{n,\gamma(n)}^{\text{LS}}$  have near-optimal accuracy and are robust to noise as described by Theorem 1, for all  $n \in \mathbb{N}$ . In this case,  $A$  is referred to as the lower bound of a Marcinkiewicz-Zygmund inequality for the doubly-indexed set of sampling functionals  $\{l_{j,\gamma(n)} : n \in \mathbb{N}, j = 1 \dots \gamma(n)\}$  [30].*

It follows from Theorem 1 that the accuracy and robustness of least squares approximations depend solely on  $A_{n,m}$ ,  $C_G$  and  $\|\mathcal{M}_m\|_{G,2}$ , which in turn do not depend on the chosen spanning set  $\Phi_n$ . However, recall from (6) that one does not directly compute  $\mathcal{F}_{n,m}^{\text{LS}}$  yet obtains the expansion coefficients via the mapping  $\mathcal{L}_{n,m}^{\text{LS}}$ . Although Theorem 1 guarantees accuracy and stability, the norm of  $\mathcal{L}_{n,m}^{\text{LS}}$  can be arbitrarily large for certain choices of spanning sets, leading to significant rounding errors. More precisely, for any  $\mathbf{d} \in \mathbb{C}^m$  we have

$$\mathcal{L}_{n,m}^{\text{LS}} \mathbf{d} = (\mathcal{M}_m \mathcal{T}_n)^\dagger \mathbf{d}, \tag{11}$$

where  $\dagger$  denotes the Moore-Penrose pseudo-inverse. Therefore,

$$\|\mathcal{L}_{n,m}^{\text{LS}}\|_{2,2} = \frac{1}{\sigma_{\min}(\mathcal{M}_m \mathcal{T}_n)} \geq \frac{1}{K \sigma_{\min}(\mathcal{T}_n)},$$

where  $\sigma_{\min}$  denotes the smallest nonzero singular value and  $K := \max_{v \in V_n, \|v\|_H=1} \|v\|_m$ . We discuss in section 2 that  $\sigma_{\min}(\mathcal{T}_n)$  is close to zero for numerically redundant spanning sets. Consequently, as elaborated on in section 3, practical algorithms implementing  $\mathcal{L}_{n,m}^{\text{LS}}$  are subject to  $\ell^2$ -regularization. The aim of this paper is to deepen our understanding of sampling strategies for numerically redundant spanning sets  $\Phi_n$ , taking into account the associated numerical effects.

### 1.3 Main contribution

The role of  $\ell^2$ -regularization in the case of a numerically redundant spanning set was first highlighted in [6, 8]. This led to an analysis of the truncated singular value decomposition (TSVD) as a means for regularizing least squares approximations. The accuracy of a TSVD approximation is described in [8, Theorem 1.3] and depends on a regularization parameter, as well as on the existence of accurate approximations with small expansion coefficients. Furthermore, the accuracy depends on two constants,  $\kappa_{M,N}^\epsilon$  and  $\lambda_{M,N}^\epsilon$ , which characterize the influence of discretization. These constants are influenced by regularization, yet in a non-transparent way.

The primary goal of this paper is to deepen our understanding of sampling for  $\ell^2$ -regularized least squares approximations. Our main contribution is the identification of a norm inequality, analogous to that of unregularized least squares approximation (9), which fully characterizes the accuracy and conditioning of these methods. The following results are part of Theorem 7 and 8.

**Theorem 2.** Consider the  $\ell^2$ -regularized least squares operator

$$\mathcal{L}_{n,m}^{RLS} : \mathbb{C}^m \rightarrow \mathbb{C}^{n'}, \quad \mathbf{d} \mapsto \arg \min_{\mathbf{x} \in \mathbb{C}^{n'}} \|\mathbf{d} - \mathcal{M}_m \mathcal{T}_n \mathbf{x}\|_2^2 + \epsilon^2 \|\mathbf{x}\|_2^2, \quad (12)$$

with associated operator  $\mathcal{F}_{n,m}^{RLS}$  defined by (7). If

$$A_{n,m}^\epsilon \|\mathcal{T}_n \mathbf{x}\|_H^2 \leq \|\mathcal{T}_n \mathbf{x}\|_m^2 + \epsilon^2 \|\mathbf{x}\|_2^2, \quad \forall \mathbf{x} \in \mathbb{C}^{n'}, \quad (13)$$

holds for some  $A_{n,m}^\epsilon > 0$ , then the error of the discrete regularized least squares approximation to  $f \in H$  satisfies

$$\|f - \mathcal{F}_{n,m}^{RLS} \mathbf{f}\|_H \leq \left( \sqrt{C_G} + \frac{(1 + \sqrt{2}) \|\mathcal{M}_m\|_{G,2}}{\sqrt{A_{n,m}^\epsilon}} \right) e_n^\epsilon(f) + \frac{1 + \sqrt{2}}{\sqrt{A_{n,m}^\epsilon}} \|\mathbf{n}\|_2,$$

where  $\mathbf{f} = \mathcal{M}_m f + \mathbf{n} \in \mathbb{C}^m$  is noisy data and

$$e_n^\epsilon(f) := \inf_{\mathbf{x} \in \mathbb{C}^{n'}} \|f - \mathcal{T}_n \mathbf{x}\|_G + \epsilon \|\mathbf{x}\|_2. \quad (14)$$

Furthermore, the absolute condition number of  $\mathcal{F}_{n,m}^{RLS}$  can be bounded by

$$\kappa_{n,m}^{RLS} \leq \frac{1 + \sqrt{2}}{\sqrt{A_{n,m}^\epsilon}}. \quad (15)$$

**Remark 4.** Here,  $\epsilon > 0$  is a regularization parameter that is of the order of  $\epsilon_{mach}$ , the working precision associated with the numerical computations, as discussed in section 3.1. This unorthodox choice of symbol for the regularization parameter emphasizes that it is small and that regularization is purely due to a finite working precision.

A couple of important conclusions are in order.

- The discretization condition (13) is a relaxation of (9); one can always find  $A_{n,m}^\epsilon \geq A_{n,m}$ . In order to see why, observe that both norm inequalities are equivalent for  $\epsilon = 0$ . In other words: it is easier to satisfy (13) than (9) and, hence, regularization can only reduce the required amount of data. After formally introducing the concept of numerical redundancy, it will become clear that this relaxation is significant only for numerically redundant spanning sets. Note that we have reduced the two constants  $\kappa_{M,N}^\epsilon$  and  $\lambda_{M,N}^\epsilon$  introduced in [8, Theorem 1.3] to a single, more transparent constant.
- The accuracy is now governed by (14) as opposed to (10). As discussed in section 2.2, this behaviour is expected when approximating with finite precision. As a result, the size of the expansion coefficients  $\|\mathbf{x}\|_2$  is an important object of study, which was also one of the main conclusions of [6, 8].
- Whereas (9) solely depends on the sampling operator  $\mathcal{M}_m$  and the approximation space  $V_n$ , (13) also depends on the spanning set  $\Phi_n$  and the regularization parameter  $\epsilon$ . These additional dependencies make its analysis significantly more complicated.

These results offer a new perspective on the influence of finite precision when working with redundant spanning sets. While finite precision leads to numerical regularization, which generally reduces accuracy compared to the best approximation, there is a benefit: regularization also decreases the amount of required information. Although predicting the exact interplay between these two effects remains challenging—particularly due to the dependence of (13) and (14) on the specific spanning set  $\Phi_n$ —this paper offers the tools to obtain a deeper understanding of practical approximation schemes.

## 1.4 Paper Overview

In section 2, we formalize the notion of numerical redundancy using ideas from low rank matrix theory and harmonic analysis. Our primary goal is to clearly identify when the effects discussed in this paper are significant. Using this framework we prove that the achievable error of a numerical approximation intrinsically depends on the achievable residual and the size of coefficients. In section 3, we motivate our focus on  $\ell^2$ -regularized approximation as a model for numerical approximation. Through a backward stability analysis we show that numerical algorithms fail to compute the expansion coefficients associated with the best approximation in the presence of numerical redundancy, yet succeed in computing  $\ell^2$ -regularized approximations. Furthermore, it is demonstrated that straightforward numerical orthogonalization cannot overcome the effects of finite-precision arithmetic. This implies that the results of this paper are relevant for a broad class of methods.

In the following part, we derive sampling theoretical results taking into account the effects of  $\ell^2$ -regularization. Section 4 formalizes how regularization relaxes the requirements for stable discretization, resulting in a decrease of the amount of data required for accurate function approximation. Our analysis is not limited to TSVD regularization, or even  $\ell^2$ -regularization; instead, we present a unified framework for regularized least squares problems with a general penalty term. In section 5, we show an additional advantage of the formulation (13): it enables constructive methods for selecting the sampling functionals  $l_{j,m}$ . Specifically, we identify an efficient random sampling distribution for  $L^2$ -approximations that takes into account the influence of regularization. Section 6 applies the results to two different settings: approximation that incorporates prior knowledge on the function to be approximated and approximation on irregular domains. In doing so, we obtain new results on sampling for Fourier extension frames. Specifically, we show that only a log-linear amount of uniformly random samples is sufficient for convergence down to machine precision in a Fourier extension frame. In contrast, an analysis that ignores the effects of regularization would suggest a need for quadratic oversampling.

## 2 Numerical redundancy

In this section, we aim to identify which spanning sets lead to significant rounding errors in the computation of expansion coefficients and how these errors affect the achievable accuracy. In order to do so, we introduce the concept of numerical redundancy. Notably, this analysis is independent of the specific discretization used.

### 2.1 Definition and links to frames theory

Consider a spanning set  $\Phi_n = \{\phi_{i,n}\}_{i=1}^{n'}$  for the approximation space  $V_n$  of dimension  $n$ , i.e.,  $\Phi_n$  satisfies  $\text{span}(\Phi_n) = V_n$ . Analytically,  $\Phi_n$  is linearly dependent only when  $n' > n$ . In this case, there exists a nonzero coefficient vector  $\mathbf{x} \in \mathbb{C}^{n'}$  that satisfies

$$\sum_{i=1}^{n'} x_i \phi_{i,n} = \mathcal{T}_n \mathbf{x} = 0,$$

i.e.,  $\mathbf{x}$  lies in the kernel of the synthesis operator  $\mathcal{T}_n$  (5). When computing numerically, the notion of linear dependency changes drastically since computations can only be performed with a finite working precision  $\epsilon_{\text{mach}}$ . A vector  $\mathbf{x}$  is stored as  $\bar{\mathbf{x}}$  where

$$\bar{\mathbf{x}} = \mathbf{x} + \Delta \mathbf{x} \quad \text{with} \quad \|\Delta \mathbf{x}\|_2 \leq \epsilon_{\text{mach}} \|\mathbf{x}\|_2.$$

This error propagates through the calculations

$$\|\mathcal{T}_n \bar{\mathbf{x}} - \mathcal{T}_n \mathbf{x}\|_H = \|\mathcal{T}_n \Delta \mathbf{x}\|_H \leq \epsilon_{\text{mach}} \|\mathcal{T}_n\|_{2,H} \|\mathbf{x}\|_2. \quad (16)$$

It follows from this simple error analysis that a nonzero vector  $\mathbf{x}$  might lie in the kernel of  $\mathcal{T}_n$  if calculations show that  $\|\mathcal{T}_n \bar{\mathbf{x}}\|_2 \leq \epsilon_{\text{mach}} \|\mathcal{T}_n\|_{2,H} \|\mathbf{x}\|_2$ .

To take into account the influence of finite precision, it is common in low rank matrix theory to introduce a numerical rank. Whereas the rank of  $\mathcal{T}_n$  equals  $n$ , i.e., the dimension of  $V_n$ , its  $\epsilon$ -rank can be defined as

$$r = \inf\{\text{rank}(\mathcal{X}_n) : \|\mathcal{T}_n - \mathcal{X}_n\|_{2,H} \leq \epsilon \|\mathcal{T}_n\|_{2,H}\}, \quad (17)$$

where the infimum is taken over all linear operators  $\mathcal{X}_n$  mapping from  $\mathbb{C}^{n'}$  to  $H$  [29]. The  $\epsilon$ -rank takes into account that, in the presence of rounding errors, the computed output  $\mathcal{T}_n \bar{\mathbf{x}}$  behaves similarly as the exact output  $\mathcal{X}_n \mathbf{x}$  of some linear operator  $\mathcal{X}_n$  that lies close to  $\mathcal{T}_n$ . Indeed, similarly to (16) one has

$$\|\mathcal{X}_n \mathbf{x} - \mathcal{T}_n \mathbf{x}\|_H \leq \epsilon \|\mathcal{T}_n\|_{2,H} \|\mathbf{x}\|_2$$

for all  $\mathcal{X}_n$  satisfying  $\|\mathcal{T}_n - \mathcal{X}_n\|_{2,H} \leq \epsilon \|\mathcal{T}_n\|_{2,H}$ . If  $r < n$  for  $\epsilon = \epsilon_{\text{mach}}$ , the operator  $\mathcal{T}_n$  is numerically rank-deficient, meaning that it is within the relative tolerance  $\epsilon_{\text{mach}}$  of an operator with rank less than  $n$ . In this case, we say that  $\Phi_n$  is numerically redundant.

**Definition 1.** A spanning set  $\Phi_n$  for the  $n$ -dimensional space  $V_n$  is called “numerically redundant” if the  $\epsilon$ -rank of its synthesis operator  $\mathcal{T}_n$  (17) is strictly less than  $n$ , where  $\epsilon = \epsilon_{\text{mach}}$  is the working precision associated with the numerical computations.

An elegant characterization of numerically redundant spanning sets follows from the field of harmonic analysis. To this end we introduce frames, which extend the concept of a Riesz basis to allow for the inclusion of linearly dependent sets. As defined by [19, Definition 1.1.1], the set  $\Phi_n$  is a frame for  $V_n$  if there exist frame bounds  $0 < A_n \leq B_n$  such that

$$A_n \|f\|_H^2 \leq \sum_{i=1}^{n'} |\langle f, \phi_{i,n} \rangle_H|^2 \leq B_n \|f\|_H^2, \quad \forall f \in V_n. \quad (18)$$

If we refer to the frame bounds  $A_n$  and  $B_n$  of  $\Phi_n$  we will always assume that they are optimal, meaning that they are the largest and smallest constants that satisfy (18), respectively.  $A_n$  and  $B_n$  always exist, since every finite set is a frame for its span [19, Corollary 1.1.3]. Furthermore, they satisfy

$$A_n = \sigma_{\min}(\mathcal{T}_n)^2 \quad \text{and} \quad B_n = \sigma_{\max}(\mathcal{T}_n)^2 \quad [19, \text{Theorem 1.3.1}], \quad (19)$$

where  $\sigma_{\min}$  and  $\sigma_{\max}$  denote the smallest and largest nonzero singular values.

From here, it follows that the lower frame bound is intrinsically linked to the size of the expansion coefficients. Namely, for any function  $f \in V_n$ , there exist expansion coefficients  $\mathbf{x} \in \mathbb{C}^{n'}$  that satisfy

$$f = \mathcal{T}_n \mathbf{x} \quad \text{and} \quad \|\mathbf{x}\|_2 \leq \|f\|_H / \sqrt{A_n}. \quad (20)$$

If the frame is linearly dependent, an infinite number of other sets of expansion coefficients describing the same function exist as well. If the lower frame bound lies close to zero no expansion can be found with reasonably sized coefficients, at least for some functions in  $V_n$ . This is precisely what happens in the case of a numerically redundant spanning set, as demonstrated by the following property.

**Property 1.** A spanning set  $\Phi_n$  is numerically redundant if and only if its frame bounds defined by (18) satisfy

$$A_n \leq \epsilon_{\text{mach}}^2 B_n.$$

*Proof.* From the extremal properties of singular values [15, Lecture 23], it follows that

$$\min_{\text{rank}(\mathcal{X}_n) < n} \|\mathcal{T}_n - \mathcal{X}_n\|_{2,H} = \sigma_{\min}(\mathcal{T}_n),$$

where the minimum is taken over all linear operators  $\mathcal{X}_n$  mapping from  $\mathbb{C}^{n'}$  to  $H$ . Combining this result with Definition 1, one can conclude that  $\Phi_n$  is numerically redundant if and only if the smallest nonzero singular value of  $\mathcal{T}_n$  is less than or equal to  $\epsilon_{\text{mach}} \|\mathcal{T}_n\|_{2,H}$ . The final result follows from (19).  $\square$

In many applications, consecutive spanning sets  $\Phi_n = \{\phi_{i,n}\}_{i=1}^{n'}$  for the approximation spaces  $\{V_n\}_{n \in \mathbb{N}}$  are finite subsequences of an infinite set  $\Psi = \{\psi_i\}_{i=1}^{\infty}$ , satisfying  $\overline{\text{span}(\Psi)} = H$ . More specifically, one chooses

$$\phi_{i,n} = \psi_i, \quad 1 \leq i \leq n', \quad \forall n \in \mathbb{N}. \quad (21)$$

Based on the properties of  $\Psi$ , one can determine whether  $\Phi_n$  is numerically redundant for sufficiently large  $n$ . In [6, section 4] this is analysed for a linearly independent infinite-dimensional frame  $\Psi$ . A set  $\Psi$  is an infinite-dimensional frame for  $H$  if there exist constants  $A, B > 0$  such that

$$A \|f\|_H^2 \leq \sum_{i=1}^{\infty} |\langle f, \psi_i \rangle_H|^2 \leq B \|f\|_H^2, \quad \forall f \in H. \quad (22)$$

Furthermore,  $\Psi$  is linearly independent if every finite subsequence is linearly independent [19, §3-4]. Note that in contrast to the finite-dimensional case, it does not hold that every infinite set is a frame for its closed span. Again, if we refer to the frame bounds  $A$  and  $B$  of  $\Psi$  we assume that they are optimal. If  $\Psi$  is a frame for  $H$ , analogously to (20) one has that for any  $f \in H$  there exist coefficients  $\mathbf{x} \in \ell^2(\mathbb{N})$  satisfying

$$f = \sum_{i=1}^{\infty} \psi_i x_i \quad \text{and} \quad \|\mathbf{x}\|_2 \leq \|f\|_H / \sqrt{A}, \quad [19, \text{Lemma 5.5.5}]. \quad (23)$$

Assuming that  $\Psi$  is a linearly independent frame, numerical redundancy can now be identified from analysing the upper and lower frame bound of  $\Phi_n$  as  $n$  increases. Following [6, Lemma 5], the upper frame bound  $B_n$  behaves nicely; it is shown that  $\{B_n\}_{n \in \mathbb{N}}$  is monotonically increasing and  $B_n \rightarrow B$ , as  $n \rightarrow \infty$ . However, the lower frame bound  $A_n$  can behave wildly; it is shown that  $\{A_n\}_{n \in \mathbb{N}}$  is monotonically decreasing and  $\inf_n A_n = 0$  if  $\Psi$  is overcomplete, which means that there exist unit-norm coefficients  $\mathbf{c} \in \ell^2(\mathbb{N})$  for which

$$\sum_{i=1}^{\infty} \psi_i c_i = 0.$$

We can conclude that if  $\Psi$  is an overcomplete frame, the lower frame bound  $A_n$  of the subsequence  $\Phi_n$  will inevitably drop below  $\epsilon_{\text{mach}}^2 \|\mathcal{T}_n\|_{2,H} = \epsilon_{\text{mach}}^2 B_n^2$  for sufficiently large  $n$ , resulting in a numerically redundant spanning set  $\Phi_n$  according to Property 1. This is not the case for subsequences of Riesz bases [19, Theorem 3.6.6 (ii)].

## 2.2 Best approximation in finite-precision arithmetic

As motivated in the previous section, when working with a finite working precision  $\epsilon_{\text{mach}}$ , the output of the operator  $\mathcal{T}_n$  can be modeled as the output of some other linear operator  $\mathcal{X}_n$  that also maps from  $\mathbb{C}^{n'}$  to  $H$  and that lies close to  $\mathcal{T}_n$

$$\|\mathcal{T}_n - \mathcal{X}_n\|_{2,H} \leq \epsilon_{\text{mach}} \|\mathcal{T}_n\|_{2,H}. \quad (24)$$

The range of  $\mathcal{X}_n$ , denoted by  $\text{R}(\mathcal{X}_n)$ , is generally not equal to  $V_n$ . Hence, the approximation space changes. To analyse this effect, we examine the error of the best approximation to a function  $f \in H$ , i.e., its orthogonal projection onto  $\text{R}(\mathcal{X}_n)$ .

**Theorem 3.** *For any  $f \in H$ , the best approximation error in the range of a linear operator  $\mathcal{X}_n : \mathbb{C}^{n'} \rightarrow H$  that satisfies (24) is bounded by*

$$\|f - \widehat{P}_n f\|_H \leq \|f - \mathcal{T}_n \mathbf{x}\|_H + \epsilon_{\text{mach}} \|\mathcal{T}_n\|_{2,H} \|\mathbf{x}\|_2, \quad \forall \mathbf{x} \in \mathbb{C}^{n'},$$

where  $\widehat{P}_n$  denotes the orthogonal projector onto  $\text{R}(\mathcal{X}_n)$ . Furthermore, using the frame bounds of  $\Phi_n$  introduced in (18), this implies

$$\|f - \widehat{P}_n f\|_H \leq \|f - P_n f\|_H + \epsilon_{\text{mach}} \sqrt{\frac{B_n}{A_n}} \|f\|_H,$$

where  $P_n$  denotes the orthogonal projector onto the approximation space  $V_n = \text{R}(\mathcal{T}_n)$ .

*Proof.* Using  $f = (f - \mathcal{T}_n \mathbf{x}) + \mathcal{T}_n \mathbf{x}$ ,  $\forall \mathbf{x} \in \mathbb{C}^{n'}$ , it follows that

$$\begin{aligned} \|f - \widehat{P}_n f\|_H &= \|(I - \widehat{P}_n) f\|_H \\ &= \|(I - \widehat{P}_n)((f - \mathcal{T}_n \mathbf{x}) + \mathcal{T}_n \mathbf{x})\|_H \\ &\leq \|I - \widehat{P}_n\|_{H,H} \|f - \mathcal{T}_n \mathbf{x}\|_H + \|(I - \widehat{P}_n) \mathcal{T}_n\|_{2,H} \|\mathbf{x}\|_2, \end{aligned}$$

where  $I : H \rightarrow H$  denotes the identity operator. The final result follows from the fact that  $I - \widehat{P}_n$  is a projector having unit operator norm, and

$$\|(I - \widehat{P}_n) \mathcal{T}_n\|_{2,H} \leq \|(I - \widehat{P}_n) \mathcal{X}_n\|_{2,H} + \|I - \widehat{P}_n\|_{H,H} \|\mathcal{T}_n - \mathcal{X}_n\|_{2,H} \leq \epsilon_{\text{mach}} \|\mathcal{T}_n\|_{2,H}.$$

The second result follows from the fact that  $P_n f \in V_n$  and, therefore, there exist coefficients  $\mathbf{c} \in \mathbb{C}^{n'}$  such that  $P_n f = \mathcal{T}_n \mathbf{c}$  with  $\|\mathbf{c}\|_2 \leq \|P_n f\|_H / \sqrt{A_n}$  (20). Hence, choosing  $\mathbf{x} = \mathbf{c}$  and using (19), it follows that

$$\|f - \widehat{P}_n f\|_H \leq \|f - \mathcal{T}_n \mathbf{c}\|_H + \epsilon_{\text{mach}} \sqrt{B_n} \|\mathbf{c}\|_2 \leq \|f - P_n f\|_H + \epsilon_{\text{mach}} \sqrt{\frac{B_n}{A_n}} \|P_n f\|_H.$$

The final result follows from  $\|P_n f\|_H \leq \|f\|_H$ .  $\square$

Theorem 3 shows that one is guaranteed that accurate approximations are computable in the presence of rounding errors, if an approximation in  $V_n$  exists that is both accurate and can be expanded in  $\Phi_n$  with reasonably sized coefficients  $\mathbf{x}$ . Furthermore, it shows that the analytical best approximation is computable up to an error of order  $\epsilon_{\text{mach}}$  if the frame bounds of  $\Phi_n$  satisfy  $A_n \approx B_n$ . On the other hand, for numerically redundant  $\Phi_n$ , we have  $\sqrt{B_n/A_n} \geq 1/\epsilon_{\text{mach}}$  such that accuracy is not guaranteed. Of course, this is only an upper bound on the error. The following lemma showcases that the bound is indeed relevant. In particular, for numerically redundant sets the upper bound can always be attained.

**Lemma 1.** *If  $\Phi_n$  is numerically redundant, there exist a linear operator  $\mathcal{X}_n : \mathbb{C}^{n'} \rightarrow H$  that satisfies (24), a nonzero function  $f \in H$ , and nonzero coefficients  $\mathbf{c} \in \mathbb{C}^{n'}$  such that*

$$\|f - \widehat{P}_n f\|_H = \|f - \mathcal{T}_n \mathbf{c}\|_H + \sigma \|\mathbf{c}\|_2,$$

where  $\sigma$  is the largest singular value of  $\mathcal{T}_n$  that is smaller than or equal to  $\epsilon_{\text{mach}} \|\mathcal{T}_n\|_{2,H}$ , implying  $0 < \sigma \leq \epsilon_{\text{mach}} \|\mathcal{T}_n\|_{2,H}$ .

*Proof.* The operator  $\mathcal{T}_n$  admits a singular value decomposition, i.e.,

$$\mathcal{T}_n = \sum_{i=1}^n \sigma_i u_i \mathbf{v}_i^*$$

where  $\{u_i\}_i$  is an orthonormal basis for  $V_n = \text{R}(\mathcal{T}_n)$  and  $\{\mathbf{v}_i\}_i$  is an orthonormal basis for  $\mathbb{C}^{n'}$ . Denote by  $r$  the number of singular values of  $\mathcal{T}_n$  that are strictly greater than  $\epsilon_{\text{mach}} \|\mathcal{T}_n\|_{2,H}$ . For numerically redundant  $\Phi_n$ , one has  $r < n$ . Consider now

$$\mathcal{X}_n = \sum_{i=1}^r \sigma_i u_i \mathbf{v}_i^*$$

and  $f = \mathcal{T}_n \mathbf{c}$  with  $\mathbf{c} = C \mathbf{v}_{r+1}$  for some nonzero  $C$ . One can check that (24) holds for this choice of  $\mathcal{X}_n$ . Furthermore,

$$\|f - \widehat{P}_n f\|_H = \|f\|_H = \|\mathcal{T}_n \mathbf{c}\|_H = C \sigma_{r+1} \|u_{r+1}\|_H = \|f - \mathcal{T}_n \mathbf{c}\|_H + C \sigma_{r+1},$$

where in the last step we add  $\|f - \mathcal{T}_n \mathbf{c}\|_H = 0$ .  $\square$

Analogous to section 2.1, one can analyse what happens as  $n \rightarrow \infty$  if the spanning sets  $\Phi_n$  for the approximation spaces  $\{V_n\}_{n \in \mathbb{N}}$  are subsequences of an infinite-dimensional set  $\Psi = \{\psi_i\}_{i=1}^\infty$  as defined by (21). If  $\Psi$  is an overcomplete frame, recall that the finite spanning sets  $\Phi_n$  are numerically redundant for sufficiently large  $n$ . This means that some functions in the approximation space cannot be represented with small expansion coefficients and, hence, it follows from Theorem 3 that accuracy of numerical approximations is not guaranteed. On the other hand, the following theorem shows that convergence down to  $\epsilon_{\text{mach}}$  is guaranteed as  $n \rightarrow \infty$ . This is related to the existence of accurate approximations with reasonably sized expansion coefficients in the set  $\Psi$ . This is an important result: even though the spanning sets  $\Phi_n$  are numerically redundant for finite  $n$ , we can still guarantee convergence of numerical approximations down to  $\epsilon_{\text{mach}}$  for every  $f \in H$  using the frame property of the infinite-dimensional set.

**Theorem 4.** *Suppose  $\{\Phi_n\}_{n \in \mathbb{N}}$  are defined by (21),  $\Psi$  satisfies (22) for some  $A, B > 0$  and  $\{\mathcal{X}_n\}_{n \in \mathbb{N}}$  is a sequence of linear operators mapping from  $\mathbb{C}^{n'}$  to  $H$  while satisfying (24) for each  $n \in \mathbb{N}$ . Then, for any  $f \in H$ ,*

$$\lim_{n \rightarrow \infty} \|f - \widehat{P}_n f\|_H \leq \epsilon_{\text{mach}} \sqrt{\frac{B}{A}} \|f\|_H,$$

where  $\widehat{P}_n$  denotes the orthogonal projector onto  $\text{R}(\mathcal{X}_n)$ .

*Proof.* Using Theorem 3, (21) and  $\lim_{n \rightarrow \infty} \|\mathcal{T}_n\|_{2,H} = \lim_{n \rightarrow \infty} \sqrt{B_n} = \sqrt{B}$  [6, Lemma 5], we find that

$$\begin{aligned} \left\| f - \widehat{P}_n f \right\|_H &\leq \|f - \mathcal{T}_n \mathbf{x}\|_H + \epsilon_{\text{mach}} \|\mathcal{T}_n\|_{2,H} \|\mathbf{x}\|_2, & \forall \mathbf{x} \in \mathbb{C}^{n'}, \\ \lim_{n \rightarrow \infty} \left\| f - \widehat{P}_n f \right\|_H &\leq \left\| f - \sum_{i=1}^{\infty} \psi_i x_i \right\|_H + \epsilon_{\text{mach}} \sqrt{B} \|\mathbf{x}\|_2, & \forall \mathbf{x} \in \ell^2(\mathbb{N}). \end{aligned}$$

Note that the infinite sum  $\sum_{i=1}^{\infty} \psi_i x_i$  converges for all  $\mathbf{x} \in \ell^2(\mathbb{N})$  since  $\Psi$  is a Bessel sequence [19, Theorem 3.2.3]. Furthermore, it follows from (23) that there exist coefficients  $\mathbf{c} \in \ell^2(\mathbb{N})$  satisfying  $f = \sum_{i=1}^{\infty} \psi_i c_i$  with  $\|\mathbf{c}\|_2 \leq \|f\|_H / \sqrt{A}$ . Hence, choosing  $\mathbf{x} = \mathbf{c}$ ,

$$\lim_{n \rightarrow \infty} \|f - \widehat{P}_n f\| \leq \left\| f - \sum_{i=1}^{\infty} \psi_i c_i \right\| + \epsilon_{\text{mach}} \sqrt{B} \|\mathbf{c}\|_2 \leq \epsilon_{\text{mach}} \sqrt{\frac{B}{A}} \|f\|_H.$$

□

### 3 Interpreting numerical approximations as $\ell^2$ -regularized approximations

In this section, we motivate why it is natural to model numerical approximations as  $\ell^2$ -regularized approximations.

#### 3.1 Error analysis with backward stability assumption

What can one reasonably expect from the output of a numerical algorithm? Due to rounding errors, recovering the exact solution is generally not possible. Moreover, even obtaining an output close to the exact solution is often unrealistic: small rounding errors can be significantly amplified by the ill-conditioning of a problem—a property that is independent of the algorithm. In numerical analysis, it is therefore common to assume / require that a numerical method is backward stable. More specifically, *a method for computing  $y = g(x)$  is called backward stable if, for any  $x$ , it produces a computed  $\widehat{y}$  with a small backward error, that is,  $\widehat{y} = g(x + \Delta x)$  for some small  $\Delta x$*  [35, section 1.5]. Here, the perturbation  $\Delta x$  does not only model rounding of the input  $x$ , but it also models the effect of rounding errors appearing throughout the calculation of  $g(x)$ . It is now natural to wonder whether backward stable algorithms output satisfying solutions in our setting. In what follows, we assume that *small* means that the perturbations can be bounded by  $\|\Delta x_i\| \leq C \epsilon_{\text{mach}} \|x_i\|$  for all inputs  $x_i$ , with  $C > 0$  a modest constant which may depend on the dimensions of  $\{x_i\}_i$ . In this case, we say that the algorithm is backward stable with stability constant  $C$ .

In essence, we are interested in computing the expansion coefficients of the orthogonal projection of a function  $f$  onto  $V_n$ , i.e.,

$$(f, \mathcal{T}_n) \mapsto \mathbf{c} = \mathcal{T}_n^\dagger f \in \arg \min_{\mathbf{x} \in \mathbb{C}^{n'}} \|f - \mathcal{T}_n \mathbf{x}\|_H^2. \quad (25)$$

Note that if  $\Phi_n$  is linearly dependent, an infinite number of other sets of expansion coefficients exist for the orthogonal projection, yet the coefficients returned by (25) have the smallest  $\ell^2$ -norm. The following theorem shows what accuracy can be expected from the output of a backward stable algorithm that implements the mapping (25). Its proof can be found in Appendix A.

**Theorem 5.** *Given a function  $f \in H$  and coefficients  $\widehat{\mathbf{c}}$  computed by a backward stable algorithm for (25) with stability constant  $C$ . Then,*

$$\|f - \mathcal{T}_n \widehat{\mathbf{c}}\|_H \leq \|f - \mathcal{T}_n \mathbf{x}\|_H + C \epsilon_{\text{mach}} (\|\mathcal{T}_n\|_{2,H} (\|\widehat{\mathbf{c}}\|_2 + \|\mathbf{x}\|_2) + 2\|f\|_H), \quad \forall \mathbf{x} \in \mathbb{C}^{n'}.$$

Furthermore, if  $\Phi_n$  is linearly independent and satisfies (18) for some  $A_n > C^2 \epsilon_{\text{mach}}^2 B_n$ , then this implies

$$\|f - \mathcal{T}_n \widehat{\mathbf{c}}\|_H \leq \|f - P_{V_n} f\|_H + C \epsilon_{\text{mach}} \left( \frac{(1 + C \epsilon_{\text{mach}}) \sqrt{B_n}}{\sqrt{A_n} - C \epsilon_{\text{mach}} \sqrt{B_n}} + \sqrt{\frac{B_n}{A_n}} + 2 \right) \|f\|_H.$$

The theorem shows that if approximations are computed using a spanning set with  $A_n \approx B_n$ , numerical rounding errors are negligible, i.e., of order  $\epsilon_{\text{mach}}$ . However, for spanning sets with  $A_n \ll B_n$  this is not the case. More specifically, accuracy can only be guaranteed if there exists a set of coefficients  $\mathbf{x}$  such that  $\|f - \mathcal{T}_n \mathbf{x}\|_H + C \epsilon_{\text{mach}} \|\mathcal{T}_n\|_{2,H} \|\mathbf{x}\|_2$  remains small, and when  $C \epsilon_{\text{mach}} \|\hat{\mathbf{c}}\|_2$  is sufficiently small where  $\hat{\mathbf{c}}$  is the computed solution. Following the discussion in section 2.2, the first condition is natural when working in finite precision, independently of which method is used to compute coefficients. On the other hand, the second condition on  $\|\hat{\mathbf{c}}\|_2$  is new and non-trivial. To see why, note that the coefficients of the best approximation  $\mathbf{c} = \mathcal{T}_n^\dagger f$  can grow arbitrarily large, in particular larger than  $\|f\|_H / (\|\mathcal{T}_n\|_H \epsilon_{\text{mach}})$  for numerically redundant spanning sets. Consequently, the norm of the computed coefficients  $\hat{\mathbf{c}}$  will likely be large as well and no accuracy can be guaranteed.

Does this mean that we cannot obtain any guarantees on the accuracy of numerical approximations when using a numerically redundant spanning set? The answer is no. However, we must slightly adapt our problem statement to reflect what is actually computed when standard solvers, such as MATLAB's `backslash`, are applied to numerically rank-deficient system. Namely, in such cases,  $\ell^2$ -regularization is used—even if the user is not explicitly aware of it. We therefore consider the regularized formulation:

$$(f, \mathcal{T}_n) \mapsto \mathbf{c} = \arg \min_{\mathbf{x} \in \mathbb{C}^{n'}} \|f - \mathcal{T}_n \mathbf{x}\|_H^2 + \epsilon^2 \|\mathbf{x}\|_2^2, \quad (26)$$

where  $\epsilon > 0$  is a regularization parameter. The mapping remains linear, and  $\mathbf{c}$  is now uniquely determined even if the spanning set  $\Phi_n$  is linearly dependent. It is important to emphasize that our use of  $\ell^2$ -regularization differs from more typical settings, e.g. in inverse problems, where it is introduced as a modeling choice to encode prior knowledge such as smoothness of the solution. In contrast, in our setting regularization is inevitable in order to ensure numerical computability. In this sense, it is not a matter of choice but a numerical necessity.

The following theorem states accuracy guarantees for backward stable algorithms, now implementing the mapping (26). The proof of Theorem 6 can again be found in Appendix A.

**Theorem 6.** *Given a function  $f \in H$  and coefficients  $\hat{\mathbf{c}}$  computed by a backward stable algorithm for (26) with stability constant  $C$ . If  $\epsilon \geq C \epsilon_{\text{mach}} \|\mathcal{T}_n\|_{2,H}$ , then*

$$\|f - \mathcal{T}_n \hat{\mathbf{c}}\|_H \leq \sqrt{2} \|f - \mathcal{T}_n \mathbf{x}\|_H + (1 + \sqrt{2}) \epsilon \|\mathbf{x}\|_2 + (1 + \sqrt{2}) C \epsilon_{\text{mach}} \|f\|_H, \quad \forall \mathbf{x} \in \mathbb{C}^{n'}.$$

We are now guaranteed to obtain accurate numerical approximations provided that there exists a set of coefficients  $\mathbf{x}$  such that  $\|f - \mathcal{T}_n \mathbf{x}\|_H + \epsilon \|\mathbf{x}\|_2$  is sufficiently small, where  $\epsilon$  is on the order of  $\epsilon_{\text{mach}}$ . This condition is natural in finite-precision arithmetic, as demonstrated in section 2.2.

### 3.2 Implicit regularization in numerical orthogonalization

From the discussion above, it may be tempting to always try to avoid numerical redundancy and obtain an orthonormal basis for  $V_n$ . Indeed, several computational methods operate with a numerically orthogonalized basis, see for example [42, 25]. But do these methods produce a substantially different approximation from that given by (26)? In this section, we show that regularization is also implicitly present in straightforward numerical orthogonalization techniques. Our goal is to convey the main ideas, though each of the pointers provided deserves further exploration. Finally, we note that Theorem 3 also suggests it is fundamentally impossible to numerically orthogonalize a redundant set without encountering issues related to finite-precision arithmetic.

For simplicity, we assume that a set of linearly independent functions  $\{\eta_1, \dots, \eta_n\}$  is given, which span the approximation space  $V_n$  with  $\dim(V_n) = n$ . One straightforward way of orthogonalizing consists of discretizing these functions on a fine grid  $\{\mathbf{t}_j\}_{j=1}^l$  and computing a factorization

$$\begin{bmatrix} \eta_1(\mathbf{t}_1)/\sqrt{l} & \dots & \eta_n(\mathbf{t}_1)/\sqrt{l} \\ \vdots & & \vdots \\ \eta_1(\mathbf{t}_l)/\sqrt{l} & \dots & \eta_n(\mathbf{t}_l)/\sqrt{l} \end{bmatrix} = A = QR, \quad (27)$$

where  $Q \in \mathbb{C}^{l \times n}$  is orthonormal and  $R \in \mathbb{C}^{n \times n}$  is full rank, for example via QR decomposition or singular value decomposition. A new basis  $\{\tilde{\eta}_1, \dots, \tilde{\eta}_n\}$  can then be obtained by solving

$$\begin{bmatrix} \tilde{\eta}_1 & \dots & \tilde{\eta}_n \end{bmatrix} R = \begin{bmatrix} \eta_1 & \dots & \eta_n \end{bmatrix}. \quad (28)$$

This basis is orthogonal with respect to the discrete inner product defined by

$$\langle f, g \rangle_l = \frac{1}{l} \sum_{j=1}^l f(\mathbf{t}_j) \overline{g(\mathbf{t}_j)}.$$

If the grid  $\{\mathbf{t}_j\}_{j=1}^l$  is sufficiently dense, the functions are also (approximately) orthonormal with respect to the inner product associated with the Hilbert space  $H$ . The basis  $\{\tilde{\eta}_j\}_{j=1}^n$  can then be used as a spanning set  $\Phi_n = \{\phi_{i,n}\}_{i=1}^n$  for least squares approximation.

Importantly, in the case of a numerically redundant set of functions  $\{\eta_1, \dots, \eta_n\}$ , the matrices  $A$  and  $R$  are heavily ill-conditioned. More specifically, their singular value profiles mimic that of the synthesis operator associated with  $\{\eta_1, \dots, \eta_n\}$ , having very small yet nonzero singular values, as discussed in section 2. Can (28) even be computed with high accuracy in such cases? As an example, we consider the QR decomposition as a factorization method for (27), such that  $R$  is upper-triangular. The accuracy of solving triangular systems of equations is analysed extensively in [34], where it is shown that the forward error depends on the Skeel condition number [49]:

$$\kappa_\infty^s(R) = \| |R^{-1}| |R| \|_\infty \leq \kappa_\infty(R) = \|R^{-1}\|_\infty \|R\|_\infty, \quad (29)$$

where  $|\cdot|$  denotes the operation of replacing each element by its absolute value. We illustrate in section 3.3 that the Skeel condition number can grow very large for numerically redundant sets. Hence, accuracy is not guaranteed. It can be hidden in practice that (28) is solved with low accuracy, since standard routines such as MATLAB's `backslash` succeed without any warning. However, due to the severe ill-conditioning of  $R$ , some form of regularization is necessarily used when computing (28).

An alternative to computing  $\{\eta_1, \dots, \eta_n\}$  explicitly using (28) consists of working with the sampled basis

$$Q = \begin{bmatrix} \tilde{\eta}_1(\mathbf{t}_1)/\sqrt{l} & \dots & \tilde{\eta}_n(\mathbf{t}_1)/\sqrt{l} \\ \vdots & & \vdots \\ \tilde{\eta}_1(\mathbf{t}_l)/\sqrt{l} & \dots & \tilde{\eta}_n(\mathbf{t}_l)/\sqrt{l} \end{bmatrix}.$$

In this case, we do not have to solve an ill-conditioned linear system; however, we can only access the basis  $\{\tilde{\eta}_1, \dots, \tilde{\eta}_n\}$  on the grid  $\{\mathbf{t}_j\}_{j=1}^l$ . As an example, we consider the accuracy of the very standard and backward stable Householder QR algorithm, which is analysed in [35, section 19.3]. Following [35, p.361], one is guaranteed to compute matrices  $\hat{Q}$  and  $\hat{R}$  such that

$$A + \Delta A = \hat{Q} \hat{R}, \quad \text{with} \quad \|\Delta a_j\|_2 \leq C \epsilon_{\text{mach}} \|a_j\|_2, \quad (30)$$

where  $C$  is a constant that depends on the dimensions of the problem and the working precision  $\epsilon_{\text{mach}}$  and  $a_j$  denotes the  $j$ -th column of  $A$ . Due to the small singular values of  $A$ , the range of  $A + \Delta A$ , and consequently the range of  $\hat{Q}$ , can differ significantly from that of  $A$ . A toy example illustrating this phenomenon is given in [51, p. 263], and a detailed study of the angle between the subspaces  $\text{R}(A)$  and  $\text{R}(A + \Delta A)$  is given in [27]. In conclusion, there are no guarantees that the computed basis functions (the columns of  $\hat{Q}$ ) span the full approximation space  $V_n$  (the range of  $A$ ).

**Remark 5.** *Observe the similarity between (30) and a truncated QR decomposition—a form of  $\ell^2$ -regularization: the range of  $\hat{Q}$  contains the singular vectors of  $A$  associated with large singular values ( $\sigma_i \gg \epsilon_{\text{mach}}$ ), while the directions associated with small singular values may be significantly perturbed or entirely missing. As a result, the best approximation cannot, in general, be computed.*

Finally, we note that there exist numerical algorithms that do succeed in computing an orthonormal basis for the whole approximation space  $V_n$ . However, in order to do so they do not explicitly orthogonalize a numerically redundant set. Instead, they rely on additional analytical knowledge. One example is the Stieltjes procedure for generating orthogonal polynomials [28], which recently gained popularity for numerical polynomial approximations in the form of the Vandermonde with Arnoldi (VwA) algorithm [18]. The orthogonalization procedure is summarized in Algorithm 1.

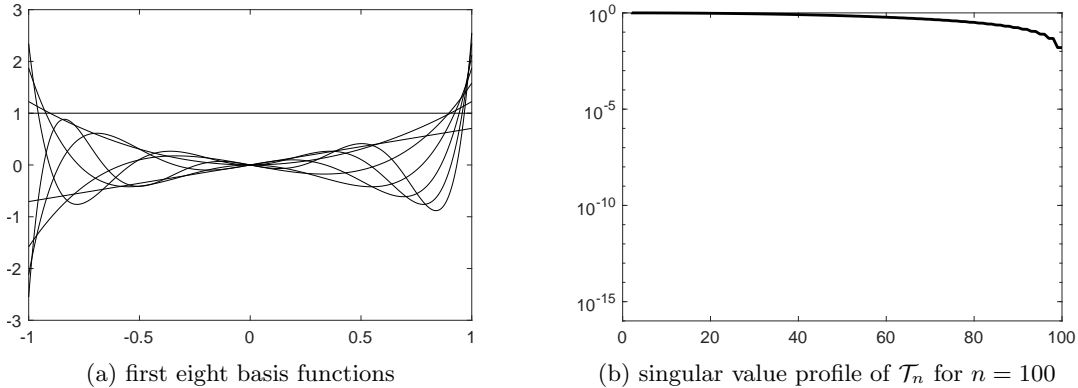


Figure 1: The Arnoldi basis associated with Stieltjes orthogonalization / the Vandermonde with Arnoldi algorithm along with the singular value profile of the associated synthesis operator. This set of functions has well behaved frame bounds, i.e.,  $A_n \approx B_n$ , in contrast to the monomials displayed in Figure 5a and 5b. Hence, the set can be numerically orthogonalized without suffering from the effects of finite precision.

---

**Algorithm 1** Stieltjes procedure for generating orthonormal polynomials.

---

```

 $\eta_1 \leftarrow 1, \tilde{\eta}_1 \leftarrow \eta_1 / \|\eta_1\|_H$ 
for  $i = 2$  to  $n$  do
   $\eta_i(\mathbf{x}) \leftarrow \mathbf{x} \tilde{\eta}_{i-1}(\mathbf{x})$ 
   $v \leftarrow \eta_i - \sum_{j=1}^{i-1} \langle \eta_i, \tilde{\eta}_j \rangle_H \tilde{\eta}_j$ 
   $\tilde{\eta}_i \leftarrow v / \|v\|_H$ 
end for
return  $\{\tilde{\eta}_1, \dots, \tilde{\eta}_n\}$ 

```

---

The success of this procedure stems from the fact that one does not orthogonalize monomials (which are numerically redundant for sufficiently large  $n$  as demonstrated on Figure 5a and 5b) yet iteratively builds “Arnoldi” basis functions  $\eta_i$  that are more suitable for orthogonalization. Indeed, Figure 1 shows that the set  $\eta_i$  defined by Algorithm 1 for the domain  $[-1, 1]$  has frame bounds satisfying  $A_n \approx B_n$ . Hence, the procedure does not suffer from the effect of finite-precision arithmetic. Stability of orthogonalization of the Arnoldi basis is analysed for a variety of domains in [53, 52]. We remark that the VwA algorithm performs discrete orthogonalization instead of the continuous orthogonalization in Algorithm 1. Furthermore, note that the algorithm can be extended to other sets of functions provided they have similar Vandermonde-like structure, as illustrated in section 3.3.

We have shown that obtaining an orthonormal basis for the full approximation space is non-trivial and can only be done numerically in specific cases, such as with the VwA algorithm. Even when an algorithm is available that avoids the effects of finite-precision arithmetic, it is natural to ask about the advantages and disadvantages of using an orthogonalized spanning set versus a regularized approximation with a redundant spanning set. Most importantly, as illustrated in section 3.3, regularization typically slows down convergence. On the other hand, it reduces the number of measurements needed for accurate approximation. To fairly compare convergence behaviour as a function of the number of samples, this phenomenon must be examined more closely, which is exactly the focus of the current paper. Additionally, orthogonalization often throws away exploitable structure. For example, in the case discussed below, the discrete least squares matrix associated with  $\Phi_n$  is a submatrix of a Fourier matrix. This structure can be leveraged to design efficient least squares methods—see, for instance, the AZ algorithm for frame approximations [22, 31]—or to enable cheaper evaluation of the approximation.

### 3.3 Numerical evidence

In section 3.1, we showed that while practical algorithms cannot reliably compute the best approximation, they can compute  $\ell^2$ -regularized approximations. Furthermore, section 3.2 demonstrated that  $\ell^2$ -regularization cannot be avoided using standard numerical orthogonalization techniques. In this

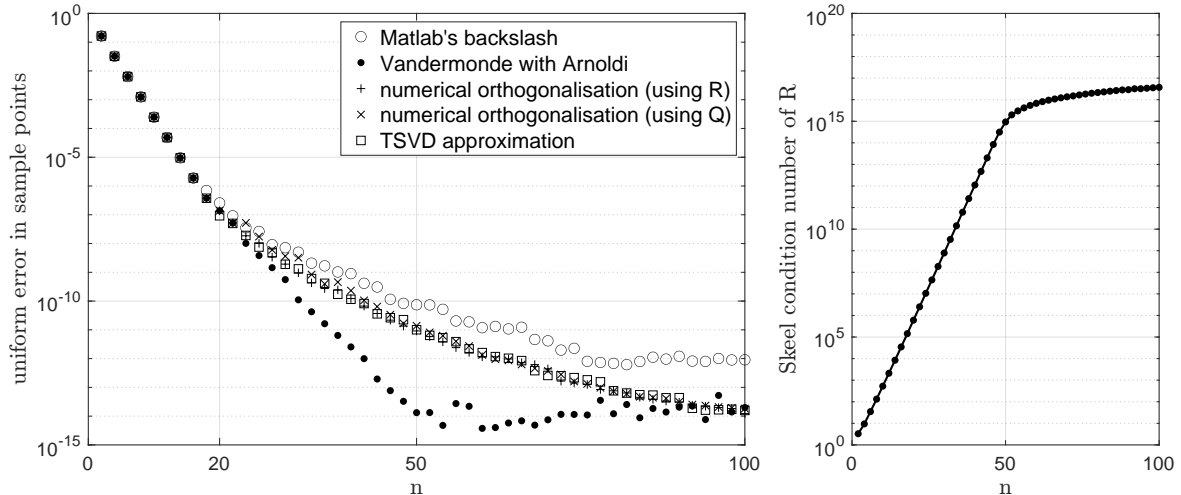


Figure 2: Approximation of  $f(x) = 1/(10-9x)$  using a Fourier extension on  $[-2, 2]$ . Left: a comparison between a regularized least squares approximation using MATLAB’s `backslash`, the Vandermonde with Arnoldi algorithm, least squares approximation using a numerically orthogonalized basis obtained via a QR decomposition, and a TSVD approximation, right: the Skeel condition number (29) of the factor  $R$ . This example demonstrates that straightforward numerical orthogonalization cannot effectively counteract the effects of finite precision, resulting in approximations that behave similarly as regularized approximations.

section, we illustrate these theoretical findings with a numerical example.

To this end, we reproduce [18, Example 3]. More specifically, we approximate the function  $f(x) = 1/(10 - 9x)$  on  $[-1, 1]$  using a Fourier extension on  $[-2, 2]$ , i.e.,

$$f(x) \approx \sum_{k=-n}^n c_k \exp(ik\pi x/2).$$

For more information on Fourier extensions, see §6.2. For now, note that this is a numerically redundant spanning set. Since  $f$  is real, this can be simplified to

$$f(x) \approx \operatorname{Re} \left( \sum_{k=0}^n x_k \exp(ik\pi x/2) \right).$$

On [18, Figure 5.1], a comparison is shown between the direct computation of a least squares fit using MATLAB’s `backslash` and the Vandermonde with Arnoldi (VwA) algorithm. The computations are based on function evaluations in 1000 Chebyshev points. Note that VwA is applicable in this setting, since the discrete least squares matrix has Vandermonde structure as described in [18, Example 3].

We add some extra methods to the comparison: approximation using a numerically orthogonalized basis obtained via a QR decomposition as described above, and a truncated singular value (TSVD) approximation, which is an explicit way of computing an  $\ell^2$ -regularized approximation. For implementational details, we refer to [18] and [32]. The results are presented in Figure 2. The VwA algorithm achieves exponential convergence, which is to be expected in  $\operatorname{span}(\Phi_n)$  [36]. On the other hand, the accuracy of the approximation computed by MATLAB’s `backslash`, as well as of the regularized and numerically orthogonalized approximations, begins to deviate from that of the best approximation starting at  $n = 20$ . This example confirms that standard routines such as MATLAB’s `backslash` and straightforward numerical orthogonalization techniques implicitly regularize the approximation problem. Furthermore, as shown in Figure 3, the spanning set  $\Phi_n$  becomes numerically redundant starting at  $n = 20$ . Hence, this illustrates that the concept of numerical redundancy accurately describes when regularization significantly impacts accuracy.

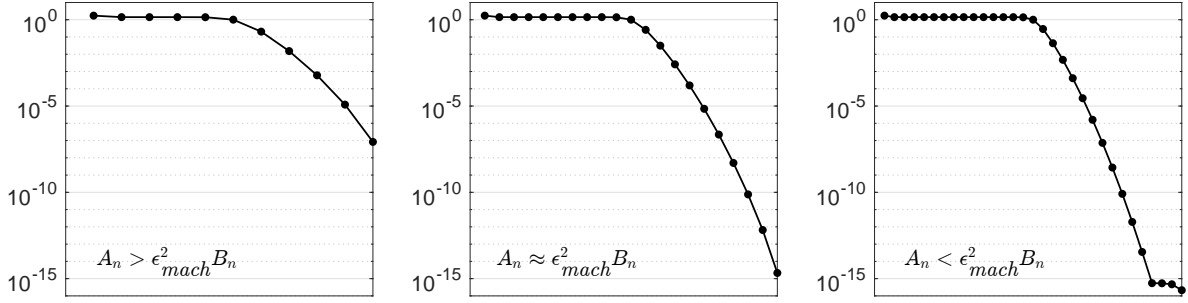


Figure 3: Singular value profile of the synthesis operator associated with  $\Phi_n = \{\text{Re}(\exp(ik\pi x/2))\}_{k=0}^n$  for  $n = 10$  (left),  $n = 20$  (middle), and  $n = 30$  (right), computed in double precision using Chebfun [26]. Analytically, the singular values decrease exponentially toward zero as  $n$  goes to infinity. The singular values are linked to the frame bounds  $A_n$  and  $B_n$  of  $\Phi_n$  via (19). The spanning set is numerically redundant starting from  $n = 20$ , i.e., when  $A_n \approx \epsilon_{\text{mach}}^2 B_n$ .

## 4 Error analysis of regularized approximations

In the previous sections, we introduced numerical redundancy and identified the numerically achievable accuracy, which differs from that of the best approximation. We also showed that numerical approximations can be interpreted as  $\ell^2$ -regularized approximations. In this section, we examine how regularization influences the errors involved in function approximation. We begin by analysing regularized least squares approximations with a more general penalty term, as our methodology naturally extends to this setting. In section 4.2, we then focus on  $\ell^2$ -regularization, particularly in the context of function approximation using a numerically redundant spanning set.

### 4.1 General penalty term

Consider the following regularized least squares operator

$$\mathcal{L}_{n,m}^{\text{RLS}} : \mathbb{C}^m \rightarrow \mathbb{C}^{n'}, \quad \mathbf{d} \mapsto \arg \min_{\mathbf{x} \in \mathbb{C}^{n'}} \|\mathbf{d} - \mathcal{M}_m \mathcal{T}_n \mathbf{x}\|_2^2 + p_\epsilon(\mathbf{x}), \quad (31)$$

with associated operator  $\mathcal{F}_{n,m}^{\text{RLS}}$  defined by (7). We assume that  $\mathcal{L}_{n,m}^{\text{RLS}}$  is well-defined, i.e., that the minimizer is unique. The penalty function  $p_\epsilon : \mathbb{C}^{n'} \rightarrow \mathbb{R}^+$  can depend on a regularization parameter  $\epsilon$ . Furthermore, we assume that  $p_\epsilon$  is even and that  $\sqrt{p_\epsilon}$  is subadditive, meaning that for all  $\mathbf{x}, \mathbf{y} \in \mathbb{C}^{n'}$  it holds that

$$\sqrt{p_\epsilon(\mathbf{x} + \mathbf{y})} \leq \sqrt{p_\epsilon(\mathbf{x})} + \sqrt{p_\epsilon(\mathbf{y})}. \quad (32)$$

Note that for any subadditive penalty term  $p_\epsilon$  (32) is automatically satisfied. Typical examples of penalty functions are related to (semi-)norms.

Section 1.2 shows that the accuracy of discrete least squares approximations depends on the norm inequality (9). The following theorem shows that the accuracy of regularized least squares approximations is dictated by a similar norm inequality

$$A_{n,m}^\epsilon \|\mathcal{T}_n \mathbf{x}\|_H^2 \leq \|\mathcal{T}_n \mathbf{x}\|_m^2 + p_\epsilon(\mathbf{x}), \quad \forall \mathbf{x} \in \mathbb{C}^{n'}. \quad (33)$$

Observe that the two inequalities are identical if  $p_\epsilon(\mathbf{x}) = 0, \forall \mathbf{x} \in \mathbb{C}^{n'}$ . Furthermore, (33) can be viewed as a relaxation of (9), because if (9) holds for some  $A_{n,m} > 0$  then (33) automatically holds for  $A_{n,m}^\epsilon = A_{n,m}$  (using the assumption that  $p_\epsilon$  is nonnegative). Analogously to Theorem 1, if the sampling operator satisfies (33) for some  $A_{n,m}^\epsilon > 0$ , then the error of the discrete regularized least squares approximation is close to optimal and the influence of measurement noise is bounded.

**Theorem 7.** *If (33) holds for some  $A_{n,m}^\epsilon > 0$ , then the error of the discrete regularized least squares approximation (31) to  $f \in H$  satisfies*

$$\|f - \mathcal{F}_{n,m}^{\text{RLS}} \mathbf{f}\|_H \leq \left( \sqrt{C_G} + \frac{(1 + \sqrt{2}) \|\mathcal{M}_m\|_{G,2}}{\sqrt{A_{n,m}^\epsilon}} \right) e_n^\epsilon(f) + \frac{1 + \sqrt{2}}{\sqrt{A_{n,m}^\epsilon}} \|\mathbf{n}\|_2,$$

where  $\mathbf{f} = \mathcal{M}_m f + \mathbf{n} \in \mathbb{C}^m$  is noisy data and

$$e_n^\epsilon(f) := \inf_{\mathbf{x} \in \mathbb{C}^{n'}} \|f - \mathcal{T}_n \mathbf{x}\|_G + \sqrt{p_\epsilon(\mathbf{x})}. \quad (34)$$

*Proof.* If  $f \notin G$ , then the right-hand side is infinite such that the bound trivially holds. Assuming  $f \in G$ , one has for any  $\mathcal{T}_n \mathbf{x} \in V_n$

$$\begin{aligned} \|f - \mathcal{F}_{n,m}^{\text{RLS}} \mathbf{f}\|_H &\leq \|f - \mathcal{T}_n \mathbf{x}\|_H + \|\mathcal{T}_n \mathbf{x} - \mathcal{F}_{n,m}^{\text{RLS}} \mathbf{f}\|_H \\ &\leq \|f - \mathcal{T}_n \mathbf{x}\|_H + \frac{1}{\sqrt{A_{n,m}^\epsilon}} \sqrt{\|\mathcal{T}_n \mathbf{x} - \mathcal{F}_{n,m}^{\text{RLS}} \mathbf{f}\|_m^2 + p_\epsilon(\mathbf{x} - \mathcal{L}_{n,m}^{\text{RLS}} \mathbf{f})} \quad (\text{using (33)}) \\ &\leq \|f - \mathcal{T}_n \mathbf{x}\|_H + \frac{1}{\sqrt{A_{n,m}^\epsilon}} \left( \|\mathcal{T}_n \mathbf{x} - \mathcal{F}_{n,m}^{\text{RLS}} \mathbf{f}\|_m + \sqrt{p_\epsilon(\mathbf{x} - \mathcal{L}_{n,m}^{\text{RLS}} \mathbf{f})} \right). \end{aligned}$$

The second term can be bounded by

$$\|\mathcal{T}_n \mathbf{x} - \mathcal{F}_{n,m}^{\text{RLS}} \mathbf{f}\|_m \leq \|\mathcal{T}_n \mathbf{x} - f\|_m + \|f - \mathcal{F}_{n,m}^{\text{RLS}} \mathbf{f}\|_m \leq \|\mathcal{T}_n \mathbf{x} - f\|_m + \|\mathbf{f} - \mathcal{M}_m \mathcal{F}_{n,m}^{\text{RLS}} \mathbf{f}\|_2 + \|\mathbf{n}\|_2,$$

while the third term can be bounded by

$$\sqrt{p_\epsilon(\mathbf{x} - \mathcal{L}_{n,m}^{\text{RLS}} \mathbf{f})} \leq \sqrt{p_\epsilon(\mathbf{x})} + \sqrt{p_\epsilon(\mathcal{L}_{n,m}^{\text{RLS}} \mathbf{f})}$$

using the fact that  $\sqrt{p_\epsilon}$  is subadditive and even. Combining these results we obtain

$$\begin{aligned} &\|\mathcal{T}_n \mathbf{x} - \mathcal{F}_{n,m}^{\text{RLS}} \mathbf{f}\|_m + \sqrt{p_\epsilon(\mathbf{x} - \mathcal{L}_{n,m}^{\text{RLS}} \mathbf{f})} \\ &\leq \|\mathcal{T}_n \mathbf{x} - f\|_m + \|\mathbf{f} - \mathcal{M}_m \mathcal{F}_{n,m}^{\text{RLS}} \mathbf{f}\|_2 + \|\mathbf{n}\|_2 + \sqrt{p_\epsilon(\mathbf{x})} + \sqrt{p_\epsilon(\mathcal{L}_{n,m}^{\text{RLS}} \mathbf{f})}, \\ &\leq (1 + \sqrt{2})(\|\mathcal{T}_n \mathbf{x} - f\|_m + \sqrt{p_\epsilon(\mathbf{x})}) + \|\mathbf{n}\|_2, \end{aligned}$$

where in the second step (31) was used, more specifically,

$$\begin{aligned} &\|\mathbf{f} - \mathcal{M}_m \mathcal{F}_{n,m}^{\text{RLS}} \mathbf{f}\|_2^2 + p_\epsilon(\mathcal{L}_{n,m}^{\text{RLS}} \mathbf{f}) \leq \|\mathbf{f} - \mathcal{M}_m \mathcal{T}_n \mathbf{x}\|_2^2 + p_\epsilon(\mathbf{x}), \\ \Rightarrow &\|\mathbf{f} - \mathcal{M}_m \mathcal{F}_{n,m}^{\text{RLS}} \mathbf{f}\|_2 + \sqrt{p_\epsilon(\mathcal{L}_{n,m}^{\text{RLS}} \mathbf{f})} \leq \sqrt{2} \left( \|\mathbf{f} - \mathcal{M}_m \mathcal{T}_n \mathbf{x}\|_2 + \sqrt{p_\epsilon(\mathbf{x})} \right), \\ \Rightarrow &\|\mathbf{f} - \mathcal{M}_m \mathcal{F}_{n,m}^{\text{RLS}} \mathbf{f}\|_2 + \sqrt{p_\epsilon(\mathcal{L}_{n,m}^{\text{RLS}} \mathbf{f})} \leq \sqrt{2} \left( \|f - \mathcal{T}_n \mathbf{x}\|_m + \|\mathbf{n}\|_2 + \sqrt{p_\epsilon(\mathbf{x})} \right). \end{aligned}$$

The final result follows from  $1 \leq \|\mathcal{M}_m\|_{G,2} < \infty$ .  $\square$

## 4.2 Numerical redundancy and $\ell^2$ -regularization

We are specifically interested in  $\ell^2$ -regularization in order to compute accurate approximations in a numerically redundant spanning set. In this case, one has  $p_\epsilon(\mathbf{x}) = \epsilon^2 \|\mathbf{x}\|_2^2$ , such that the discretization condition (33) becomes

$$A_{n,m}^\epsilon \|\mathcal{T}_n \mathbf{x}\|_H^2 \leq \|\mathcal{T}_n \mathbf{x}\|_m^2 + \epsilon^2 \|\mathbf{x}\|_2^2, \quad \forall \mathbf{x} \in \mathbb{C}^{n'}. \quad (35)$$

### 4.2.1 Absolute condition number

When using  $\ell^2$ -regularization, the operator  $\mathcal{F}_{n,m}^{\text{RLS}}$  is linear. We can easily characterize its absolute condition number using  $A_{n,m}^\epsilon$ .

**Theorem 8.** *If (35) holds for some  $A_{n,m}^\epsilon > 0$ , then the absolute condition number of the regularized least squares operator  $\mathcal{F}_{n,m}^{\text{RLS}}$  defined by (7) and (31) with  $p_\epsilon(\mathbf{x}) = \epsilon^2 \|\mathbf{x}\|_2^2$  satisfies*

$$\kappa_{n,m}^{\text{RLS}} \leq \frac{1 + \sqrt{2}}{\sqrt{A_{n,m}^\epsilon}}.$$

*Proof.* Since  $\mathcal{F}_{n,m}^{\text{RLS}}$  is a linear operator, one has

$$\begin{aligned} (\kappa_{n,m}^{\text{RLS}})^2 &= \sup_{\mathbf{d} \in \mathbb{C}^m} \frac{\|\mathcal{F}_{n,m}^{\text{RLS}} \mathbf{d}\|_H^2}{\|\mathbf{d}\|_2^2} \\ &\leq \left( \sup_{\mathbf{d} \in \mathbb{C}^m} \frac{\|\mathcal{F}_{n,m}^{\text{RLS}} \mathbf{d}\|_H^2}{\|\mathcal{F}_{n,m}^{\text{RLS}} \mathbf{d}\|_m^2 + \epsilon^2 \|\mathcal{L}_{n,m}^{\text{RLS}} \mathbf{d}\|_2^2} \right) \left( \sup_{\mathbf{d} \in \mathbb{C}^m} \frac{\|\mathcal{F}_{n,m}^{\text{RLS}} \mathbf{d}\|_m^2 + \epsilon^2 \|\mathcal{L}_{n,m}^{\text{RLS}} \mathbf{d}\|_2^2}{\|\mathbf{d}\|_2^2} \right), \end{aligned}$$

where  $\mathcal{L}_{n,m}^{\text{RLS}}$  is defined by (31) with  $p_\epsilon(\mathbf{x}) = \epsilon^2 \|\mathbf{x}\|_2^2$ . The first factor can be bounded by  $1/A_{n,m}^\epsilon$  using (35). To bound the second factor, note that following the definition of  $\mathcal{L}_{n,m}^{\text{RLS}}$  one has

$$\|\mathbf{d} - \mathcal{M}_m \mathcal{F}_{n,m}^{\text{RLS}} \mathbf{d}\|_2^2 + \epsilon^2 \|\mathcal{L}_{n,m}^{\text{RLS}} \mathbf{d}\|_2^2 \leq \|\mathbf{d} - \mathcal{M}_m \mathcal{T}_n \mathbf{x}\|_2^2 + \epsilon^2 \|\mathbf{x}\|_2^2,$$

for all  $\mathbf{x} \in \mathbb{C}^{n'}$ . If we consider  $\mathbf{x} = \mathbf{0}$ , it follows that

$$\begin{aligned} \|\mathbf{d} - \mathcal{M}_m \mathcal{F}_{n,m}^{\text{RLS}} \mathbf{d}\|_2^2 + \epsilon^2 \|\mathcal{L}_{n,m}^{\text{RLS}} \mathbf{d}\|_2^2 &\leq \|\mathbf{d}\|_2^2 \\ \|\mathbf{d} - \mathcal{M}_m \mathcal{F}_{n,m}^{\text{RLS}} \mathbf{d}\|_2 + \epsilon \|\mathcal{L}_{n,m}^{\text{RLS}} \mathbf{d}\|_2 &\leq \sqrt{2} \|\mathbf{d}\|_2 && \text{(via } (a+b)^2 \leq 2(a^2 + b^2), \forall a, b \in \mathbb{R}^+) \\ \|\mathcal{M}_m \mathcal{F}_{n,m}^{\text{RLS}} \mathbf{d}\|_2 - \|\mathbf{d}\|_2 + \epsilon \|\mathcal{L}_{n,m}^{\text{RLS}} \mathbf{d}\|_2 &\leq \sqrt{2} \|\mathbf{d}\|_2 && \text{(reverse triangle inequality)} \\ \frac{\|\mathcal{F}_{n,m}^{\text{RLS}} \mathbf{d}\|_m + \epsilon \|\mathcal{L}_{n,m}^{\text{RLS}} \mathbf{d}\|_2}{\|\mathbf{d}\|_2} &\leq 1 + \sqrt{2} \\ \frac{\|\mathcal{F}_{n,m}^{\text{RLS}} \mathbf{d}\|_m^2 + \epsilon^2 \|\mathcal{L}_{n,m}^{\text{RLS}} \mathbf{d}\|_2^2}{\|\mathbf{d}\|_2^2} &\leq (1 + \sqrt{2})^2 && \text{(via } a^2 + b^2 \leq (a+b)^2, \forall a, b \in \mathbb{R}^+) \end{aligned}$$

□

#### 4.2.2 Interpretation of the discretization condition

One might wonder how big the influence of the penalty term is for small  $\epsilon$ . To this end, consider a numerically redundant spanning set  $\Phi_n$  with frame bounds  $A_n$  and  $B_n$ , and choose  $\epsilon = \epsilon_{\text{mach}} \|\mathcal{T}_n\|_{2,H} = \epsilon_{\text{mach}} \sqrt{B_n}$  for simplicity. Recall that the results of section 3.1 show that it should be taken slightly larger in practice. As follows from (19), the smallest nonzero singular value of  $\mathcal{T}_n$  is equal to  $\sqrt{A_n}$ . Using Property 1, this means that there exist  $\mathbf{x} \in \mathbb{C}^{n'}$  for which

$$\|\mathcal{T}_n \mathbf{x}\|_H^2 = A_n \|\mathbf{x}\|_2^2 \leq \epsilon_{\text{mach}}^2 B_n \|\mathbf{x}\|_2^2 = \epsilon^2 \|\mathbf{x}\|_2^2$$

and, hence, for these sets of expansion coefficients (35) is automatically satisfied for  $A_{n,m}^\epsilon = 1$ . More generally, (35) is automatically satisfied for any  $\mathbf{x} \in \mathbb{C}^{n'}$  satisfying  $\|\mathcal{T}_n \mathbf{x}\|_H \leq \epsilon \|\mathbf{x}\|_2$ . This reflects the idea that regularization makes the effective approximation space smaller.

What happens in the case of an orthonormal spanning set? Such a set satisfies Parseval's identity:  $\|\mathcal{T}_n \mathbf{x}\|_H = \|\mathbf{x}\|_2$ . Therefore, (35) is equivalent to

$$(A_{n,m}^\epsilon - \epsilon^2) \|v\|_H^2 \leq \|v\|_m^2, \quad \forall v \in V_n, \quad (36)$$

which is a negligible relaxation compared to (9) for small  $\epsilon$ . Hence, the penalty term only has a big influence on the discretization condition when  $\Phi_n$  is numerically redundant.

To show how the penalty term affects the discretization condition in a simple setting, consider a basis  $\Phi_n$  with sampling operator  $\mathcal{M}_m$ , and suppose we add a new function  $\psi$  to the basis. Intuitively, increasing the approximation space would require more samples to preserve stability. However, if  $\psi$  can be approximated to machine precision by  $\Phi_n$ , then the space hasn't really grown numerically. As Boyd discusses in [17, Section 16.6], such additions are effectively invisible on a computer. In this case, no extra samples are needed. This can be substantiated using (35), which accounts for finite precision, while the standard condition (9) in general no longer holds (i.e.,  $A_{n,m} = 0$  for the augmented basis).

**Lemma 2** (Augmented basis). *Given a basis  $\Phi_n$  with  $V_n = \text{span}(\Phi_n)$ , and a sampling operator  $\mathcal{M}_m$  satisfying*

$$\|v\|_H^2 = \|v\|_m^2, \quad \forall v \in V_n. \quad (37)$$

Suppose we augment this basis with one additional function  $\psi$ . If

$$\inf_{v \in V_n} \|\psi - v\|_G \leq \epsilon / (\|\mathcal{M}_m\|_{G,2} + \sqrt{C_G}), \quad (38)$$

then

$$\frac{1}{2} \|\mathcal{T}\mathbf{x}\|_H^2 \leq \|\mathcal{T}\mathbf{x}\|_m^2 + \epsilon^2 \|\mathbf{x}\|_2^2, \quad \forall \mathbf{x} \in \mathbb{C}^{n+1}, \quad (39)$$

where  $\mathcal{T}$  is the synthesis operator associated with  $\Phi_n \cup \{\psi\}$ .

*Proof.* Define

$$\mathcal{T}\mathbf{x} = \sum_{i=1}^n x_i \phi_{i,n} + x_{n+1} \psi =: f + x_{n+1} \psi.$$

For any  $g \in V_n$ , it holds that

$$\|\mathcal{T}\mathbf{x}\|_H = \|f + x_{n+1} \psi\|_H \leq \|f + g\|_H + \|x_{n+1} \psi - g\|_H.$$

Furthermore, using (37),

$$\|f + g\|_H = \|f + g\|_m \leq \|f + x_{n+1} \psi\|_m + \|g - x_{n+1} \psi\|_m = \|\mathcal{T}\mathbf{x}\|_m + \|g - x_{n+1} \psi\|_m.$$

Hence,

$$\begin{aligned} \|\mathcal{T}\mathbf{x}\|_H &\leq \|\mathcal{T}\mathbf{x}\|_m + \|x_{n+1} \psi - g\|_m + \|x_{n+1} \psi - g\|_H \\ \|\mathcal{T}\mathbf{x}\|_H &\leq \|\mathcal{T}\mathbf{x}\|_m + (\|\mathcal{M}_m\|_{G,2} + \sqrt{C_G}) \|x_{n+1} \psi - g\|_G. \end{aligned}$$

Since the above holds for any  $g \in V_n$ , it follows from (38) that

$$\|\mathcal{T}\mathbf{x}\|_H \leq \|\mathcal{T}\mathbf{x}\|_m + \epsilon |x_{n+1}|.$$

Using  $(a+b)^2 \leq 2(a^2 + b^2)$ , this leads to

$$\|\mathcal{T}\mathbf{x}\|_H^2 \leq (\|\mathcal{T}\mathbf{x}\|_m + \epsilon |x_{n+1}|)^2 \leq 2(\|\mathcal{T}\mathbf{x}\|_m^2 + \epsilon^2 |x_{n+1}|^2) \leq 2(\|\mathcal{T}\mathbf{x}\|_m^2 + \epsilon^2 \|\mathbf{x}\|_2^2).$$

□

### 4.2.3 Common methods for $\ell^2$ -regularization

The choice  $p_\epsilon(\mathbf{x}) = \epsilon^2 \|\mathbf{x}\|_2^2$  is also known as Tikhonov regularization. Another popular method for  $\ell^2$ -regularization is the truncated singular value decomposition (TSVD). This type of regularization slightly differs from Tikhonov regularization, yet a near-optimal solution is returned in the following sense: for any input data  $\mathbf{d} \in \mathbb{C}^m$  the computed coefficients  $\mathcal{L}_{n,m} \mathbf{d}$  satisfy

$$\|\mathbf{d} - \mathcal{M}_m \mathcal{T}_n \mathcal{L}_{n,m} \mathbf{d}\|_2 + \epsilon \|\mathcal{L}_{n,m} \mathbf{d}\|_2 \leq C_{\mathcal{L}} (\|\mathbf{d} - \mathcal{M}_m \mathcal{T}_n \mathbf{x}\|_2 + \epsilon \|\mathbf{x}\|_2), \quad \forall \mathbf{x} \in \mathbb{C}^{n'}, \quad (40)$$

for some  $C_{\mathcal{L}} \geq 1$ . With only a minor adjustment to the proof of Theorem 7, it follows immediately that the approximation error can be bounded by

$$\|f - \mathcal{F}_{n,m} \mathbf{f}\|_H \leq \left( \sqrt{C_G} + \frac{(1 + C_{\mathcal{L}}) \|\mathcal{M}_m\|_{G,2}}{\sqrt{A_{n,m}^\epsilon}} \right) e_n^\epsilon(f) + \frac{1 + C_{\mathcal{L}}}{\sqrt{A_{n,m}^\epsilon}} \|\mathbf{n}\|_2. \quad (41)$$

For completeness, we show that TSVD regularization indeed satisfies (40). The same result follows from combining [22, Lemma 3.3] and [8, Theorem 3.8].

**Lemma 3** (TSVD regularization). *The operator*

$$\mathcal{L}_{n,m}^{TSVD} : \mathbb{C}^m \rightarrow \mathbb{C}^{n'}, \quad \mathbf{d} \mapsto (\mathcal{M}_m \mathcal{T}_n)_\epsilon^\dagger \mathbf{d},$$

where  $(\cdot)_\epsilon^\dagger$  denotes the Moore-Penrose inverse after truncation of the singular values below a threshold  $\epsilon$ , satisfies (40) for  $C_{\mathcal{L}} = 2$ .

*Proof.* Define  $T := \mathcal{M}_m \mathcal{T}_n$ . It holds that

$$\begin{aligned} T(T)_\epsilon^\dagger &= \sum_i \mathbf{u}_i \sigma_i \mathbf{v}_i^* \sum_{\sigma_i \geq \epsilon} \mathbf{v}_i \frac{1}{\sigma_i} \mathbf{u}_i^* = \sum_{\sigma_i \geq \epsilon} \mathbf{u}_i \mathbf{u}_i^*, \\ (T)_\epsilon^\dagger T &= \sum_{\sigma_i \geq \epsilon} \mathbf{v}_i \frac{1}{\sigma_i} \mathbf{u}_i^* \sum_i \mathbf{u}_i \sigma_i \mathbf{v}_i^* = \sum_{\sigma_i \geq \epsilon} \mathbf{v}_i \mathbf{v}_i^*, \end{aligned}$$

where  $\mathbf{u}_i$ ,  $\sigma_i$  and  $\mathbf{v}_i$  are the left singular vectors, singular values and right singular vectors of  $T$ , respectively. Hence,  $T(T)_\epsilon^\dagger$  and  $(T)_\epsilon^\dagger T$  are orthogonal projections onto  $\text{span}(\{\mathbf{u}_i \mid \sigma_i \geq \epsilon\})$  and  $\text{span}(\{\mathbf{v}_i \mid \sigma_i \geq \epsilon\})$ , respectively. Using  $\mathbf{d} = (\mathbf{d} - T\mathbf{x}) + T\mathbf{x}$ ,  $\forall \mathbf{x} \in \mathbb{C}^{n'}$ , it follows from here that

$$\begin{aligned} \|\mathbf{d} - T(T)_\epsilon^\dagger \mathbf{d}\|_2 &= \|(I - T(T)_\epsilon^\dagger)((\mathbf{d} - T\mathbf{x}) + T\mathbf{x})\|_2 \\ &\leq \|I - T(T)_\epsilon^\dagger\|_{2,2} \|\mathbf{d} - T\mathbf{x}\|_2 + \|(I - T(T)_\epsilon^\dagger)T\|_{2,2} \|\mathbf{x}\|_2, \\ &\leq \|\mathbf{d} - T\mathbf{x}\|_2 + \epsilon \|\mathbf{x}\|_2, \end{aligned}$$

where  $I : \mathbb{C}^m \rightarrow \mathbb{C}^m$  is the identity operator. Similarly,

$$\begin{aligned} \epsilon \|(T)_\epsilon^\dagger \mathbf{d}\|_2 &= \epsilon \|(T)_\epsilon^\dagger ((\mathbf{d} - T\mathbf{x}) + T\mathbf{x})\|_2 \\ &\leq \epsilon \|(T)_\epsilon^\dagger\|_{2,2} \|\mathbf{d} - T\mathbf{x}\|_2 + \epsilon \|(T)_\epsilon^\dagger T\|_{2,2} \|\mathbf{x}\|_2, \\ &\leq \|\mathbf{d} - T\mathbf{x}\|_2 + \epsilon \|\mathbf{x}\|_2. \end{aligned}$$

□

## 5 Random sampling for $L^2$ -approximations

The question naturally arises: how can one construct a sampling operator that satisfies the regularized norm inequality (35)? To address this question, we draw inspiration from the unregularized case. Recently, Cohen and Migliorati [21] introduced an elegant strategy to generate random pointwise samples that satisfy (9) for least squares fitting. This approach, reviewed in section 5.1, is closely related to the concept of *leverage scores*, which are used to subsample tall-and-skinny matrices in a discrete setting. Leverage score sampling is a well-established technique in numerical linear algebra and machine learning. Moreover, an extension of leverage scores, known as *ridge leverage scores*, has been developed specifically for regularized settings. Using a continuous analogue of these scores, we present a sampling strategy for  $\ell^2$ -regularized function approximation in section 5.2. In section 5.3, a general framework is given for the analysis of the effects of regularization given a numerically redundant spanning set. Throughout the whole section, we work under the mild assumption that for any  $\mathbf{x}$  in the domain of  $V_n$ , there exists a  $v \in V_n$  such that  $v(\mathbf{x}) \neq 0$ .

### 5.1 Results without regularization

In [20, 21] random sampling for discrete least squares approximation of unknown functions  $f : X \rightarrow \mathbb{R}$  living in  $H = L^2(X, d\rho)$  is analysed, where  $X \subset \mathbb{R}^d$  and  $\rho$  is a given probability measure on  $X$ . The analysis is based on the observation that the norm inequality (9) is equivalent to a spectral bound

$$A_{n,m} G_n \preceq G_{n,m}, \quad (42)$$

where  $\preceq$  denotes the Loewner order. Here,  $G_{n,m}$  and  $G_n$  are the discrete and continuous Gram matrices representing the operators  $(\mathcal{M}_m \mathcal{U}_n)^* (\mathcal{M}_m \mathcal{U}_n)$  and  $\mathcal{U}_n^* \mathcal{U}_n$ , respectively, where  $\mathcal{U}_n$  is the synthesis operator associated with any set of functions  $\Psi_n$  satisfying  $\text{span}(\Psi_n) = V_n$ . We stress that this equivalence holds for any such set  $\Psi_n$ , not only for the chosen spanning set  $\Phi_n$ . However, if one considers an orthonormal set  $\Psi_n = \{\psi_i\}_{i=1}^n$ , the analysis simplifies significantly. In this case, one has  $G_n = I$  and  $A_{n,m}$  is simply related to the smallest eigenvalue of  $G_{n,m}$ .

As explained in [21, Proof of Theorem 2.1], suppose one uses a sampling operator  $\mathcal{M}_m$  based on random pointwise samples

$$l_{j,m} : f \mapsto \sqrt{w(\mathbf{x}_j)/mf(\mathbf{x}_j)}, \quad \mathbf{x}_j \stackrel{\text{iid}}{\sim} \mu, \quad (43)$$

where the sampling measure  $d\mu$  and weight function  $w$  satisfy  $w d\mu = d\rho$ . Then,  $G_{n,m}$  can be written as  $\sum_{j=1}^m X_j$  where  $X_j$  are i.i.d. copies of the random matrix  $X(\mathbf{x})$  with

$$(X(\mathbf{x}))_{k,l} := \frac{1}{m} w(\mathbf{x}) \overline{\psi_k(\mathbf{x})} \psi_l(\mathbf{x}), \quad k, l = 1 \dots n,$$

where  $\mathbf{x}$  is distributed according to  $\mu$ . The smallest eigenvalue of  $G_{n,m}$  can now be bounded from below with high probability using a matrix concentration bound that solely depends on the number of samples  $m$  and the maximum of the quantity

$$\|X(\mathbf{x})\|_2 = \frac{1}{m} w(\mathbf{x}) \sum_{i=1}^n |\psi_i(\mathbf{x})|^2 = \frac{1}{m} w(\mathbf{x}) k_n(\mathbf{x}),$$

where we defined

$$k_n(\mathbf{x}) := \sum_{i=1}^n |\psi_i(\mathbf{x})|^2. \quad (44)$$

This definition assumes that  $\Psi_n$  is orthonormal. However, it is independent of the specific choice of the orthonormal set  $\Psi_n$ ; the function  $k_n$  only depends on  $V_n = \text{span}(\Psi_n)$  and the probability density  $\rho$ . The function  $k_n$  has been analysed in the field of classical analysis long before its introduction in the analysis of discrete least squares problems. In classical analysis, it is known as the inverse of the *Christoffel function* [44]. Furthermore, its discrete analogue is known as *leverage scores*, which are frequently used in randomized numerical linear algebra and machine learning, see e.g. [41, §2].

This reasoning led to the following sampling result, which is a restatement of [25, Lemma 2.1].

**Theorem 9.** [25, Lemma 2.1] *Consider the sampling operator  $\mathcal{M}_m$  defined by the sampling functionals (43). Let  $\gamma > 0$  and*

$$m \geq 9.25 \|wk_n\|_{L^\infty(X)} \log(2n/\gamma), \quad (45)$$

*then (9) is satisfied for  $A_{n,m} = 1/2$  with probability at least  $1 - \gamma$ .*

Can we optimize the sampling distribution  $\mu$  such that the required number of samples in Theorem 9 is minimized? The following key observation was first highlighted in [21]. Observe that  $\{\sqrt{w}\psi_i\}_{i=1}^n$  is an  $L^2(X, d\mu)$  orthonormal basis for  $\sqrt{w}V_n$  and, therefore,  $\int_X w(\mathbf{x}) k_n(\mathbf{x}) d\mu = n$ . As a consequence, we know that  $\|wk_n\|_{L^\infty(X)} \geq n$ . Consider now the sampling distribution

$$w(\mathbf{x}) = \frac{n}{k_n(\mathbf{x})}, \quad \text{such that} \quad d\mu = \frac{k_n(\mathbf{x})}{n} d\rho. \quad (46)$$

This sampling distribution satisfies  $\|wk_n\|_{L^\infty(X)} = n$  and, hence, minimizes the right-hand side of (45). One can easily check that (46) indeed describes a probability density since  $\int_X k_n(\mathbf{x}) d\rho = n$  and  $k_n(\mathbf{x}) > 0$ . The following result is a restatement of [21, Theorem 2.1].

**Corollary 1.** *Consider the sampling operator  $\mathcal{M}_m$  defined by the sampling functionals (43) with  $d\mu$  as defined by (46). Let  $\gamma > 0$  and*

$$m \geq 9.25n \log(2n/\gamma),$$

*then (9) is satisfied for  $A_{n,m} = 1/2$  with probability at least  $1 - \gamma$ .*

It follows that the sampling distribution (46) requires only  $\mathcal{O}(n \log(n))$  samples for accurate least squares fitting with high probability. As a result, the amount of required data is nearly optimal, where “optimal” corresponds to the case of interpolation with  $m = n$ . For a summary of optimality benchmarks and probabilistic error analyses, we refer to [25, sections 1 and 2]. Also, we note that considerable efforts have been made to obtain  $\mathcal{O}(n)$  sampling strategies, see e.g. [1, section 8] and references therein. However, these methods are no longer purely random, which diverges from the focus of this section.

## 5.2 Results with $\ell^2$ -regularization

We now turn to random sampling for discrete  $\ell^2$ -regularized least squares approximations to unknown functions  $f : X \rightarrow \mathbb{R}$  living in  $H = L^2(X, d\rho)$ . Analogously to (42), observe that (35) is equivalent to

$$A_{n,m}G_n \preceq G_{n,m} + \epsilon^2 I. \quad (47)$$

An important difference compared to section 5.1 is the dependence on the chosen spanning set  $\Phi_n$ . In this case, we are bound to the choice  $\Psi_n = \Phi_n$ , i.e.,  $G_{n,m}$  and  $G_n$  represent the operators  $(\mathcal{M}_m \mathcal{T}_n)^*(\mathcal{M}_m \mathcal{T}_n)$  and  $\mathcal{T}_n^* \mathcal{T}_n$ , respectively, where  $\mathcal{T}_n$  is the synthesis operator associated with the spanning set  $\Phi_n$ .

Similar spectral bounds have been analysed before in the setting of randomized algorithms [11, 12, 13, 48] using analogous techniques as the ones described in section 5.1. In this case, a continuous analogue of the  $\epsilon$ -ridge leverage scores [11, Definition 1] is of interest

$$k_n^\epsilon(\mathbf{x}) := \sum_{i=1}^n \frac{\sigma_i^2}{\sigma_i^2 + \epsilon^2} |u_i(\mathbf{x})|^2, \quad (48)$$

where  $\sigma_i$  and  $u_i(\mathbf{x})$  are the singular values and left singular vectors, evaluated at  $\mathbf{x}$ , associated with the synthesis operator  $\mathcal{T}_n$ . We refer to (48) as the inverse of the numerical Christoffel function.

The following properties are easily derived:  $k_n^0 = k_n$  and  $k_n^\epsilon \leq k_n$ . Furthermore, whereas  $k_n$  solely depends on the subspace  $V_n$  and the  $L^2(X, d\rho)$ -norm,  $k_n^\epsilon$  also depends on the chosen spanning set  $\Phi_n$  and the regularization parameter  $\epsilon$ . Another important difference is that  $\int_X k_n(\mathbf{x}) d\rho = n$ , but

$$\int_X k_n^\epsilon(\mathbf{x}) d\rho = \sum_{i=1}^n \frac{\sigma_i^2}{\sigma_i^2 + \epsilon^2} =: n^\epsilon, \quad (49)$$

where we call the quantity  $n^\epsilon$  the numerical dimension. In the discrete context,  $n^\epsilon$  is also known as the effective dimension or the effective degrees of freedom [11]. It satisfies  $n^\epsilon \leq n$  and it is a decreasing function of the regularization parameter  $\epsilon$ .

Using very similar techniques as [12, proof of Lemma 6], we can prove the following sampling result. The reworked proof can be found in Appendix B.<sup>1</sup>

**Theorem 10.** *Consider the sampling operator  $\mathcal{M}_m$  defined by the sampling functionals (43). Assuming  $\epsilon > 0$  and  $\|G_n\|_2 \geq \epsilon^2$ , let  $\gamma \in (0, 1)$  and*

$$m \geq \frac{32}{3} \|wk_n^\epsilon\|_\infty \log(16n^\epsilon/\gamma),$$

where  $\|wk_n^\epsilon\|_\infty = \sup_{\mathbf{x} \in X} |w(\mathbf{x})k_n^\epsilon(\mathbf{x})|$ , then (35) is satisfied for  $A_{n,m}^\epsilon = 1/2$  with probability at least  $1 - \gamma$ .

Following a similar reasoning as in section 5.1, we again consider the sampling distribution with

$$w(\mathbf{x}) = \frac{n^\epsilon}{k_n^\epsilon(\mathbf{x})}, \quad \text{such that} \quad d\mu = \frac{k_n^\epsilon(\mathbf{x})}{n^\epsilon} d\rho. \quad (50)$$

It follows from  $\int_X k_n^\epsilon(\mathbf{x}) d\rho = n^\epsilon$  that (50) is indeed a well-defined sampling distribution.

**Corollary 2.** *Consider the sampling operator  $\mathcal{M}_m$  defined by the sampling functionals (43) with  $d\mu$  as defined by (50). Assuming  $\epsilon > 0$  and  $\|G_n\|_2 \geq \epsilon^2$ , let  $\gamma \in (0, 1)$  and*

$$m \geq \frac{32}{3} n^\epsilon \log(16n^\epsilon/\gamma),$$

then (35) is satisfied for  $A_{n,m}^\epsilon = 1/2$  with probability at least  $1 - \gamma$ .

<sup>1</sup>We believe a result involving the  $L^\infty(X)$ -norm might be true, as in Theorem 9. However, the proof of Theorem 10 relies on the matrix concentration inequality given in [12, Lemma 27] which requires the use of the uniform norm.

It is worthwhile to interpret the differences between the results laid out in section 5.1 and those in this section. Using Theorem 1 the sampling strategy proposed in Corollary 1 results in a least squares approximation with

$$\|f - \mathcal{F}_{n,m}^{\text{LS}} \mathbf{f}\|_H \leq C \inf_{v \in V_n} \|f - v\|_G \quad (51)$$

using

$$m \geq Cn \log(n) \quad (52)$$

samples, with high probability and assuming the data  $\mathbf{f}$  is noiseless. On the other hand, it follows from Theorem 2 that the sampling strategy proposed in Corollary 2 results in a regularized least squares approximation with

$$\|f - \mathcal{F}_{n,m}^{\text{RLS}} \mathbf{f}\|_H \leq C \inf_{\mathbf{x} \in \mathbb{C}^{n'}} \|f - \mathcal{T}_n \mathbf{x}\|_G + \epsilon \|\mathbf{x}\|_2 \quad (53)$$

using

$$m \geq Cn^\epsilon \log(n^\epsilon) \quad (54)$$

samples, again with high probability and assuming the data  $\mathbf{f}$  is noiseless. In these statements the constant  $C > 0$  is generic and may change with each occurrence. These results demonstrate that regularization generally decreases the achievable accuracy, yet also decreases the amount of data required to obtain a near-best approximation. Furthermore, the numerical dimension  $n^\epsilon$  in regularized approximations serves a similar role as the dimension  $n$  in unregularized approximations.

Note that in practice one typically has  $n^\epsilon = \mathcal{O}(n)$  such that (52) and (54) are asymptotically equivalent as  $n \rightarrow \infty$ . This suggests that the gain in data efficiency achieved through regularization is generally limited to a constant factor when samples are drawn from the optimal distributions proposed in Corollary 1 and 2. On the other hand, regularization can have a more substantial influence on the required sample complexity if one cannot choose the sample distribution. Since  $k_n$  can differ significantly from  $k_n^\epsilon$ , the required number of samples drawn from a specific distribution  $\mu$  may vary considerably depending on whether or not the effects of regularization are accounted for, as described in Theorems 9 and 10. An illustration of this phenomenon are the results of section 6.2.2 for Fourier extension frames.

### 5.3 Behaviour of $n^\epsilon$ and $k_n^\epsilon$

For approximation with numerically redundant spanning sets, we are specifically interested in the setting where  $\epsilon$  is of the order of a finite working precision  $\epsilon_{\text{mach}}$  associated with the numerical computations. It is important to gain intuition in the impact of the penalty term, i.e., whether the numerical dimension  $n^\epsilon$  differs significantly from  $n$  and the behaviour of  $k_n^\epsilon$  differs significantly from the behaviour of  $k_n$ , for small regularization parameters  $\epsilon$ .

Following [6] and section 2, numerically redundant spanning sets  $\Phi_n$  that form a subsequence of a linearly independent overcomplete frame  $\Psi$  are of particular interest. For these sets, regularized approximations are guaranteed to converge down to  $\epsilon_{\text{mach}}$  accuracy, see e.g. Theorem 4. As discussed in section 2.1, the singular values of the synthesis operator associated with such spanning sets lie within  $[A_n, B_n]$ , where  $A_n \rightarrow 0$  as  $n \rightarrow \infty$  and  $B_n < B$ . Here,  $A_n$  and  $B_n$  denote the frame bounds of  $\Phi_n$ , and  $B$  denotes the upper frame bound of the infinite-dimensional frame  $\Psi$ . Figure 4 illustrates a typical singular value profile of a synthesis operator  $\mathcal{T}_n$  associated with a spanning set that is a subsequence of a frame  $\Psi$  with  $A = B = 1$ . Notably, whereas the spectrum of the synthesis operator associated with  $\Psi$  is contained within  $\{0\} \cup [A, B]$ , the finite synthesis operator  $\mathcal{T}_n$  has spurious eigenvalues in  $(0, A)$ , which arise due to spectral pollution [24].

One can split the singular value profile into different regimes, by identifying  $i_1$  and  $i_2$  such that

$$\sigma_i^2 \geq 1 - \epsilon^2 \text{ for } i \leq i_1 \quad (55)$$

and

$$\sigma_i^2 \leq \epsilon^2 \text{ for } i > i_2. \quad (56)$$

The region in between  $i_1$  and  $i_2$  is often referred to as the *plunge region* [23]. These regions have a different influence on the numerical dimension  $n^\epsilon$  and the maximum of the inverse numerical Christoffel function  $k_n^\epsilon$ , as quantified in the following theorem, of which the proof can be found in Appendix C.

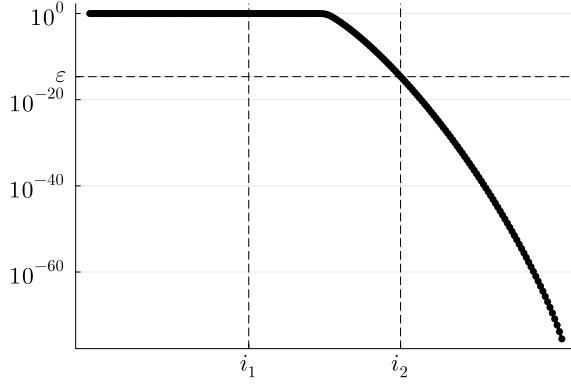


Figure 4: A typical singular value profile of the synthesis operator  $\mathcal{T}_n$  associated with a subsequence (21) of a linearly independent overcomplete frame with frame bounds  $A = B = 1$ . The singular value profile can be analysed by splitting it in three regions, where  $\sigma_i^2 \geq 1 - \epsilon^2$  for  $i \leq i_1$  and  $\sigma_i^2 \leq \epsilon^2$  for  $i > i_2$ . The region in between  $i_1$  and  $i_2$  is often referred to as the plunge region.

**Theorem 11.** *Given  $i_1$  and  $i_2$  satisfying (55) and (56), then*

$$n^\epsilon \leq i_2 + S_{tail} \quad (57)$$

and

$$\frac{1}{2} k_n^{trunc}(\mathbf{x}) \leq k_n^\epsilon(\mathbf{x}) \leq k_n^{trunc}(\mathbf{x}) + S_{tail} \max_{i_2 < i \leq n} |u_i(\mathbf{x})|^2, \quad (58)$$

where  $S_{tail} = \sum_{i=i_2+1}^n (\sigma_i/\epsilon)^2$  and  $k_n^{trunc}(\mathbf{x}) = \sum_{i=1}^{i_2} |u_i(\mathbf{x})|^2$ . Furthermore, if  $\Phi_n$  is linearly independent and uniformly bounded,  $\|\phi_{i,n}\|_\infty \leq 1$  ( $1 \leq i \leq n$ ), then

$$\|k_n^\epsilon\|_\infty \leq \frac{n}{1 - \epsilon^2} + ((i_2 - i_1) + S_{tail}) \max_{i_1 < i \leq n} \|u_i\|_\infty^2. \quad (59)$$

Foremost, it becomes clear that regularization decreases the importance of small singular values and the associated basis functions  $u_i$ . For the numerical dimension, it follows from Theorem 11 that  $S_{tail} = \sum_{i=i_2+1}^n (\sigma_i/\epsilon)^2$  is an important quantity. This quantity heavily depends on the decay of the singular values. For instance, if they are exponentially decaying with a rate that is independent of  $n$ , one has  $S_{tail} \leq C$  for varying  $n$ . In this case, the numerical dimension scales with  $i_2$ . In practice, the decay of the singular values typically has a minor dependence on  $n$ , see e.g. section 6.2.1, such that  $S_{tail}$  grows slowly with  $n$ . Furthermore, we find that the basis functions  $u_i$  associated with small singular values indeed have a smaller impact on (58) and (59) than those associated to large singular values. This effect can be considerable, as illustrated in section 6.2.2 for the Fourier extension frame, where  $k_n = \mathcal{O}(n^2)$  while  $k_n^\epsilon = \mathcal{O}(n \log(n))$ .

The reasoning above could give the impression that the behaviour of the basis functions  $u_i$  associated to small singular values ( $i > i_2$ ) is insignificant. According to (58) this is not generally true; only if these functions are sufficiently bounded, is the inverse numerical Christoffel function  $k_n^\epsilon$  guaranteed to behave like the inverse Christoffel function  $k_n^{trunc}$  associated to the set  $\{u_i\}_{i=1}^{i_2}$ . In the discrete setting, the latter is referred to as the leverage scores associated to the best rank- $i_2$  space [11]. This distinction is important for practical purposes, since  $k_n^{trunc}$  is computable to high accuracy using  $\epsilon_{mach}$  precision, while computing  $k_n^\epsilon$  and  $k_n$  requires extended precision.

## 6 Applications

### 6.1 Approximating with known singularities

An approximation problem typically stems from an underlying problem in science or engineering where expert knowledge on its solution is available. It is, however, non-trivial to incorporate this knowledge into an efficient numerical scheme. One way to do this is by adding extra basis functions to the spanning set, which capture the known properties of the function to be approximated. This forces us

to compute with non-standard bases that are typically numerically redundant. We choose a simple example to illuminate the principles, noting that they hold much more generally.

Suppose our goal is to approximate

$$f(x) = J_{1/2}(x+1) + \frac{1}{x^2+1}, \quad x \in [-1, 1] \quad (60)$$

where  $J_{1/2}$  denotes the Bessel function of the first kind of order  $1/2$ . It is known from asymptotic analysis that  $J_{1/2}(x+1) \sim \sqrt{x+1}$  as  $x \rightarrow -1$ , which can be taken into account by working with a spanning set

$$\Phi_n = \{\varphi_i\}_{i=1}^{n/2} \cup \{\psi_i\}_{i=1}^{n/2}, \quad \text{where } \psi_i = w\varphi_i, \quad (61)$$

assuming  $n$  is even. The functions  $\varphi_i$  are standard (smooth) basis functions, while the singular behaviour is represented by the weight function  $w$ . For  $w \in L^\infty(-1, 1)$ , this spanning set is a subsequence of an overcomplete linearly independent frame with frame bounds  $A = 1 + \text{ess inf}_{x \in (-1, 1)} |w(x)|^2$  and  $B = 1 + \text{ess sup}_{x \in (-1, 1)} |w(x)|^2$  [6, Example 3]. Hence, following section 2.1,  $\Phi_n$  is numerically redundant for sufficiently large  $n$ . For further analysis and usecases of this type of spanning sets we refer to [6] and references therein. For the approximation of  $f$  (60), we choose  $\varphi_i$  equal to the Legendre polynomial of degree  $i-1$  and  $w(x) = \sqrt{(x+1)/2}$ . In this case,  $\Phi_n$  is a subsequence of a frame with frame bounds  $A = 1$  and  $B = 2$ .

### 6.1.1 Numerical redundancy in action

On Figure 5, the approximation of  $f$  (60) for three different spanning sets is shown: Legendre polynomials, monomials, and the Legendre + Weighted Legendre spanning set defined by (61). Figures 5a and 5b display the first eight elements of the spanning sets along with the singular value profile of their associated synthesis operator for  $n = 100$ . The Legendre basis functions are orthonormal, such that all singular values of the synthesis operator are equal to 1. In contrast, the monomials and the Legendre + Weighted Legendre spanning set are both numerically redundant for sufficiently large  $n$ . However, a clear qualitative difference exists between these two sets. As can be seen on Figure 5a, the monomials look increasingly more alike as their degree increases, such that high-degree monomials are indistinguishable when using finite precision. As a result, all singular values of the synthesis operator are exponentially decaying. The Legendre + Weighted Legendre spanning set contains half of the Legendre basis augmented with weighted Legendre functions. Hence, in contrast to the monomial basis, a large portion of the set is well-distinguishable. As a result, the synthesis operator has many singular values  $\sigma_i \approx 1$ , combined with exponentially decaying singular values. This matches the singular value profile described in section 5.3.

On Figure 5c and 5d, the  $L^2$ -norm of the approximation error and the  $L^2$ -norm of the expansion coefficients are displayed for the approximation of  $f$  using a truncated singular value decomposition (TSVD) solver with  $\epsilon = 10 \epsilon_{\text{mach}}^{\text{dp}}$ , where  $\epsilon_{\text{mach}}^{\text{dp}}$  denotes the working precision associated with IEEE double precision floating point numbers. The approximations are computed using 5000 Legendre points. Both the Legendre basis and the monomials span the space of polynomials up to degree  $n-1$  and, therefore, theoretically exhibit the same algebraic rate of convergence for the approximation of  $f$ . However, the expansion coefficients of the monomial approximations blow up, such that the error of the numerically computed approximation stagnates, following the results of section 2.2. On the other hand, the approximation in the Legendre + weighted Legendre spanning set converges exponentially. The norm of the expansion coefficients initially grows, yet expansions with modest coefficient exist as  $n \rightarrow \infty$ , guaranteeing accurate numerical approximations. This is to be expected, since  $\Phi_n$  is a subsequence of an infinite-dimensional linearly independent frame, see e.g. Theorem 4.

This comparison demonstrates that numerical redundancy should not be viewed as a drawback; rather, allowing it enables the development of non-standard computational methods. The inclusion of weighted polynomials, for instance, leads to a significant improvement in the speed of convergence. However, not all numerically redundant sets are advantageous for computational purposes. For example, in the monomial basis no accurate solutions with bounded coefficients exist, resulting in a stagnation of the error of the best approximation in finite-precision arithmetic.

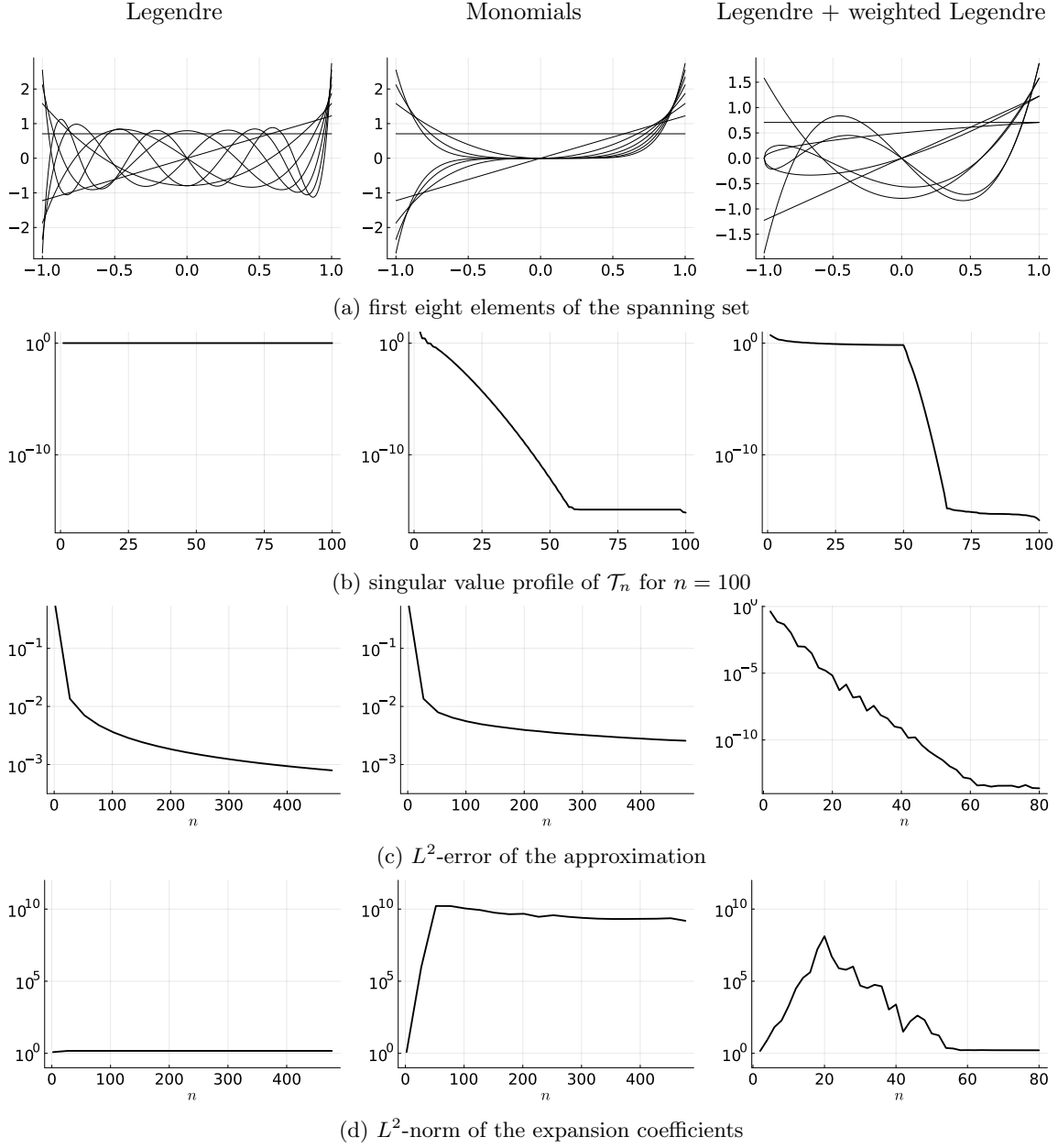


Figure 5: Comparison between approximating with Legendre polynomials up to degree  $n-1$ , monomials up to degree  $n-1$  and the Legendre + weighted Legendre spanning set defined by (61) for the approximation of  $f(x) = J_{1/2}(x+1) + 1/(x^2+1)$  using a TSVD solver with  $\epsilon = 10 \epsilon_{\text{mach}}^{\text{dp}}$ .

### 6.1.2 Analysis of deterministic point sets

Deterministic sample sets can be analysed by identifying the largest  $A_{n,m}^\epsilon$  for which the norm inequality

$$A_{n,m}^\epsilon \|\mathcal{T}_n \mathbf{x}\|_H^2 \leq \|\mathcal{T}_n \mathbf{x}\|_m^2 + \epsilon^2 \|\mathbf{x}\|_2^2, \quad \forall \mathbf{x} \in \mathbb{C}^n$$

holds. An error bound on the discrete regularized least squares approximation then follows from Theorem 2. Observe that one can determine  $A_{n,m}^\epsilon$  by computing the smallest generalized eigenvalue  $\lambda$  of

$$(G_{n,m} + \epsilon^2 I) \mathbf{v} = \lambda G_n \mathbf{v}, \quad (62)$$

where  $G_{n,m}$  and  $G_n$  represent the operators  $(\mathcal{M}_m \mathcal{T}_n)^* (\mathcal{M}_m \mathcal{T}_n)$  and  $\mathcal{T}_n^* \mathcal{T}_n$ , respectively. We compare this to the largest  $A_{n,m}$  for which the norm inequality

$$A_{n,m} \|v\|_H^2 \leq \|v\|_m^2, \quad \forall v \in V_n$$

holds, which corresponds to the smallest generalized eigenvalue  $\lambda$  of

$$G_{n,m} \mathbf{v} = \lambda G_n \mathbf{v}. \quad (63)$$

The constant  $A_{n,m}$  results in an error bound on the discrete least squares approximation via Theorem 1.

How should one choose sample points for approximation in the spanning set defined by (61)? Intuitively, it is clear that we need sample points related to the smooth behaviour of  $\varphi_i$  and sample points related to the singular behaviour of  $w$ . For the first we use Legendre points, while for the latter we use sample points that are exponentially clustered towards  $x = -1$ . Using a structured point set such as Legendre points is advantageous as it creates structured subblocks within the discrete least squares matrix. This structure can be exploited to increase the computational efficiency of solving the least squares problem, as demonstrated by the AZ algorithm for frame approximations [22, 31]. Moreover, exponentially clustered points have been found effective for least squares approximation of functions with branch point singularities [33].

The two-parameter plots on Figure 6 show  $1/\sqrt{A_{m,n}}$ ,  $1/\sqrt{A_{m,n}^\epsilon}$ , and the uniform approximation error of the TSVD approximation to  $f = J_{1/2}(x+1) + 1/(x^2+1)$  in  $\Phi_n$  (61) with  $n = 80$ , for a varying number of Legendre points and exponentially clustered sample points. The regularization parameter equals  $\epsilon = 10 \epsilon_{\text{mach}}^{\text{dp}}$ , where  $\epsilon_{\text{mach}}^{\text{dp}}$  denotes the working precision associated with IEEE double precision floating point numbers. From Figure 5c, we know that the best approximation to  $f$  in the Legendre + weighted Legendre spanning set is of the order of machine precision. Following Theorem 1 and Theorem 2, both  $1/\sqrt{A_{m,n}}$  and  $1/\sqrt{A_{m,n}^\epsilon}$  give an indication of the error of the discrete least squares approximation. We can conclude that  $A_{n,m}^\epsilon$  accurately predicts the behaviour of the approximation error, while  $A_{n,m}$  overestimates the amount of samples that are needed for accurate numerical approximation.

## 6.2 Approximating on irregular domains

Approximating a function on an irregular domain  $D \subset \mathbb{R}^d$  is required for many computational problems, yet an orthonormal or Riesz basis is generally unknown for such a domain. Therefore, numerical methods often resort to working with an orthonormal basis defined on a bounding box surrounding  $D$ . Crucially, this set of functions does not form an orthonormal basis for the underlying domain  $D$ , but it does constitute an overcomplete frame, referred to as an *extension frame*. As discussed in section 2.1, a subsequence of an overcomplete frame inevitably becomes numerically redundant as its size increases and, hence, practical approximations are subject to  $\ell^2$ -regularization. Approximating on an irregular domain is, therefore, a typical scenario in which numerical redundancy arises.

As a toy example for the behaviour of extension frames, we will analyse a one-dimensional Fourier extension frame. More specifically, for approximation on  $[-W, W]$  with  $W < 1/2$  one can use the Fourier basis on the extension  $[-1/2, 1/2]$ , i.e.,

$$\phi_{k,n} = \exp(2\pi i x k), \quad -(n-1)/2 \leq k \leq (n-1)/2 \quad (64)$$

for odd  $n$ . Smooth functions, not necessarily periodic on  $[-W, W]$ , can be approximated in  $V_n = \text{span}(\Phi_n)$  with exponential convergence [36]. The numerical convergence behaviour, taking into account the influence of regularization, is extensively analysed in [9].

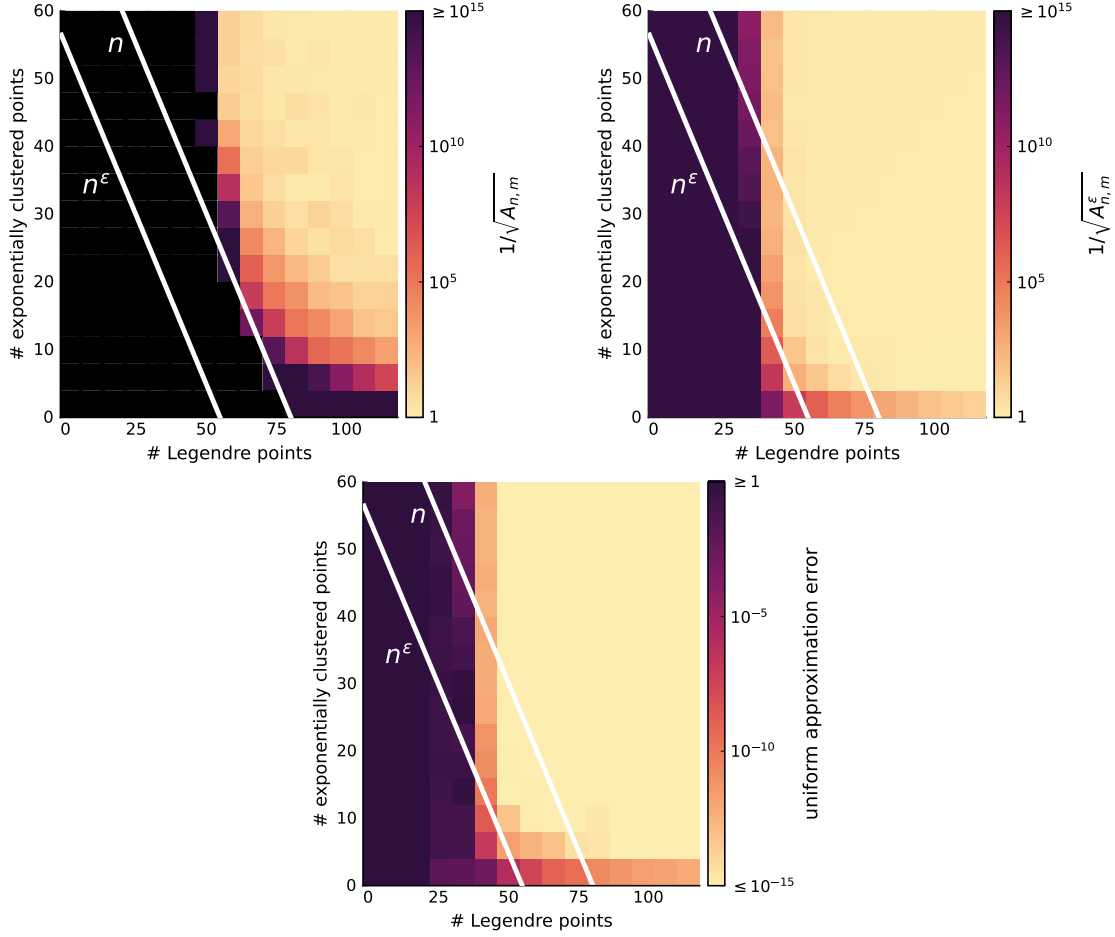


Figure 6: Analysis of the Legendre + weighted Legendre spanning set defined by (61) for  $n = 80$ . Left:  $1/\sqrt{A_{n,m}}$ , right:  $1/\sqrt{A_{n,m}^\epsilon}$  for  $\epsilon = 10 \epsilon_{\text{mach}}^{\text{dp}} \approx 2 \times 10^{-15}$ , bottom: the uniform approximation error of the TSVD approximation of  $f(x) = J_{1/2}(x+1) + 1/(x^2+1)$  with truncation threshold  $\epsilon$ . The black squares correspond to  $A_{n,m} = 0$ . The white lines mark when the total number of samples equals  $n = 80$  or  $n^\epsilon \approx 54.8$ , the numerical dimension. We conclude that  $A_{n,m}^\epsilon$  accurately predicts the behaviour of the approximation error, while  $A_{n,m}$  overestimates the amount of samples that are needed for accurate numerical approximation.

In this section, we analyse how regularization affects the required amount of data for accurate approximation using the results from section 5, which focus on random pointwise sampling. The associated analysis outlined in section 5.3 depends heavily on a good understanding of the singular values and the singular vectors associated to the synthesis operator  $\mathcal{T}_n$ . For many spanning sets, little is known about this; the singular vectors of the Fourier extension frame are, however, related to discrete prolate spheroidal wave functions (DPSWFs), which have been analysed extensively in the field of signal processing. For a detailed explanation of this connection, see [40, section 3.1]. DPSWFs are an indispensable tool for bandlimited extrapolation, introduced and thoroughly analysed by Slepian and his collaborators during their time at Bell Labs [50]. In this setting, a notion of numerical dimension is not new, see e.g. [39] and [23, section 2.3]

We note that many high-dimensional approximation algorithms assume that the target function is defined on a tensor-product domain. A common example is surrogate model construction in uncertainty quantification. In practice, however, variables are often correlated, or the forward model may be infeasible on parts of the domain. As a result, the approximation effectively becomes a Fourier or polynomial frame approximation, as explained in [7]. To fully understand such methods, including their information-based complexity, a detailed analysis of the role of regularization is essential. The analysis in this section offers an initial step towards a deeper understanding of these approaches.

### 6.2.1 Numerical dimension

In the case of pointwise random sampling, the required number of samples for accurate regularized least squares approximation scales with  $n^\epsilon \log(n^\epsilon)$ , as stated in Theorem 10. Here,  $n^\epsilon$  denotes the numerical dimension. This theorem assumes that the samples are drawn randomly from a (near-)optimal sampling distribution defined by (50). The numerical dimension  $n^\epsilon$  thus plays a similar role for regularized approximation as the dimension  $n$  for unregularized approximation. The following theorem formalizes the dependence of  $n^\epsilon$  on  $n$ ,  $W$  and  $\epsilon$  for the one-dimensional Fourier extension frame.

**Theorem 12.** *For the spanning set defined by (64),*

$$i_2 = \lceil 2nW \rceil + 2 + \frac{2}{\pi^2} \log\left(\frac{8}{\epsilon^2}\right) \log(4n) \quad (65)$$

*satisfies (56). For this choice of  $i_2$ , one has*

$$S_{tail} \leq \frac{2}{\pi^2} \log(4n) \quad (66)$$

*such that the numerical dimension  $n^\epsilon$  can be bounded by*

$$n^\epsilon \leq \lceil 2nW \rceil + 2 + \frac{2}{\pi^2} \left( \log\left(\frac{8}{\epsilon^2}\right) + 1 \right) \log(4n). \quad (67)$$

*Proof.* Note that  $\sigma_i(\mathcal{T}_n)^2$  equals the  $i$ -th eigenvalue of the Gram matrix  $G_n$ , representing the operator  $\mathcal{T}_n^* \mathcal{T}_n$ . Furthermore,  $G_n$  is exactly the *prolate matrix* [38, eq. (1)]. Therefore,  $\sigma_i(\mathcal{T}_n)^2 = \lambda_{i-1}$ , for all  $i = 1, \dots, n$ , where the latter is analysed in [38]. It follows from [38, Corollary 1] that (56) holds for (65). Moreover, (66) can be deduced by [38, Corollary 2]. The final result is a consequence of Theorem 11.  $\square$

A numerical verification of Theorem 12 is shown on Figure 7 for  $n = 141$  and  $\epsilon = 10 \epsilon_{\text{mach}}^{\text{sp}} \approx 10^{-6}$  and  $\epsilon = 10 \epsilon_{\text{mach}}^{\text{dp}} \approx 2 \times 10^{-15}$ , where  $\epsilon_{\text{mach}}^{\text{sp}}$  and  $\epsilon_{\text{mach}}^{\text{dp}}$  denote the working precision associated with IEEE single and double precision floating point numbers, respectively. Note that the computation of  $n^\epsilon$  is done in extended precision, such that the singular values  $\sigma_i$  can be computed with a working precision significantly smaller than  $\epsilon$ . For implementational details, we refer to [32]. Both the theory and the numerical verification show that the numerical dimension essentially scales as  $2nW$ . This formalizes the intuition that increased redundancy, i.e., smaller  $W$ , results in a reduced amount of required information. Observe that  $n^\epsilon = \mathcal{O}(n)$ , such that asymptotically the number of samples needed for regularized and unregularized approximation is similar, namely  $\mathcal{O}(n \log(n))$ .

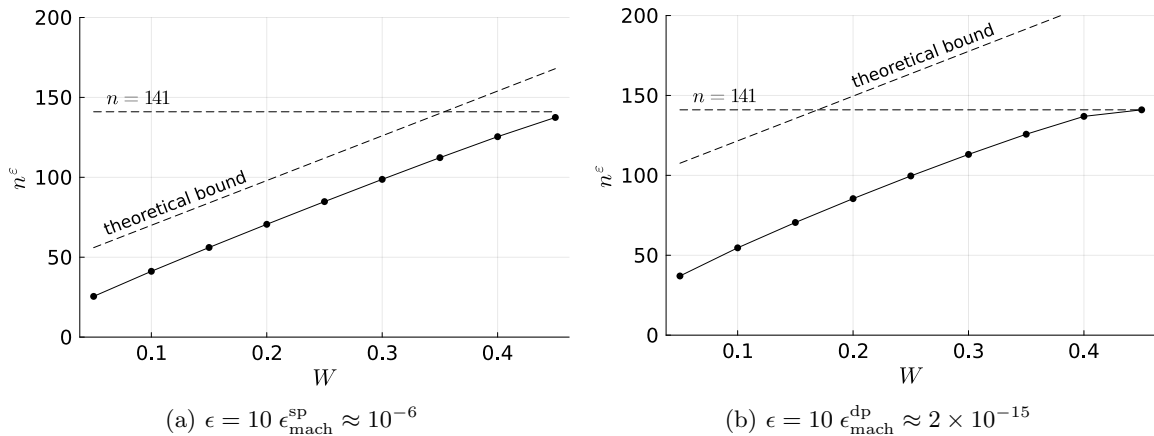


Figure 7: The numerical dimension  $n^\epsilon$  for the one-dimensional Fourier extension frame (64) as a function of the domain parameter  $W$ , for  $n = 141$ . The dashed lines illustrate  $n^\epsilon \leq n = 141$  and the theoretical bound  $n^\epsilon \leq \lceil 2nW \rceil + 2 + \frac{2}{\pi^2} (\log(8/\epsilon^2) + 1) \log(4n)$  stated in Theorem 12.

### 6.2.2 Uniformly random sampling

For many applications, one cannot freely choose the sample distribution. Another interesting question to answer in this regard is how many uniformly random samples are needed for accurate approximation. As follows from Theorems 9 and 10 for  $w = 1$ , this number is proportional to the maximum of the inverse Christoffel function  $k_n$  and the inverse numerical Christoffel function  $k_n^\epsilon$  for unregularized and regularized least squares fitting, respectively. The following theorem shows that  $\|k_n\|_{L^\infty[-W,W]} = \mathcal{O}(n^2)$ .

**Theorem 13.** *For the spanning set defined by (64) with  $W < 1/2$ , the Christoffel function satisfies*

$$\|k_n\|_{L^\infty[-W,W]} \geq k_n(W) \sim n^2 \frac{\pi}{2} \cot(W\pi) \quad \text{as } n \rightarrow \infty.$$

*Proof.* In [54] a related kernel is being analysed as a means to determine the pointwise convergence behaviour of Fourier extensions. More specifically, in [54], the kernel  $K_N(x, y)$  is analysed, which we relate to the inverse Christoffel function  $k_n$  in our setting via

$$k_n(x) = K_n(x/W, x/W)/W, \quad x \in [-W, W].$$

We can, therefore, restrict ourselves to the analysis of  $K_N(x, x)$  for  $x \in [-1, 1]$ . The result can now be obtained by combining [54, Theorem 4.1] with [54, eq. 8], which is valid for large degree  $n$  and for  $x \in [1 - \delta, 1]$  for some  $\delta > 0$ . After expanding all quantities for large  $n$  and plugging in  $x = 1$ , one obtains the asymptotic result via lengthy but straightforward calculations. The inequality  $\|k_n\|_{L^\infty[-W,W]} \geq k_n(W)$  holds since  $\|k_n\|_{L^\infty[-W,W]} = \|k_n\|_\infty$ .  $\square$

The inverse numerical Christoffel function  $k_n^\epsilon$  can be bounded using (59), which depends on the size of the plunge region  $i_2 - i_1$  and  $S_{\text{tail}}$ . The latter is shown to be  $\mathcal{O}(\log(n))$  in Theorem 12. The following theorem proves that the size of the plunge region is  $\mathcal{O}(\log(n))$  as well.

**Theorem 14.** *For the spanning set defined by (64),*

$$i_1 = \lfloor 2nW \rfloor - 1 - \frac{2}{\pi^2} \log\left(\frac{8}{\epsilon^2}\right) \log(4n) \quad (68)$$

*satisfies (55). Moreover, the maximum of  $k_n^\epsilon$  can be bounded by*

$$\|k_n^\epsilon\|_\infty \leq \frac{n}{1 - \epsilon^2} + \left(4 + \frac{2}{\pi^2} \left(2 \log\left(\frac{8}{\epsilon^2}\right) + 1\right) \log(4n)\right) \max_{i_1 < i \leq n} \|u_i\|_\infty^2. \quad (69)$$

*Proof.* Similarly as for the proof of Theorem 12, observe that  $\sigma_i(\mathcal{T}_n)^2 = \lambda_{i-1}$ , for all  $i = 1, \dots, n$ , where the latter is analysed in [38]. It follows from [38, Corollary 1] that (55) holds for (68). By combining the results from Theorem 12 with (59) and (68), we arrive at (69).  $\square$

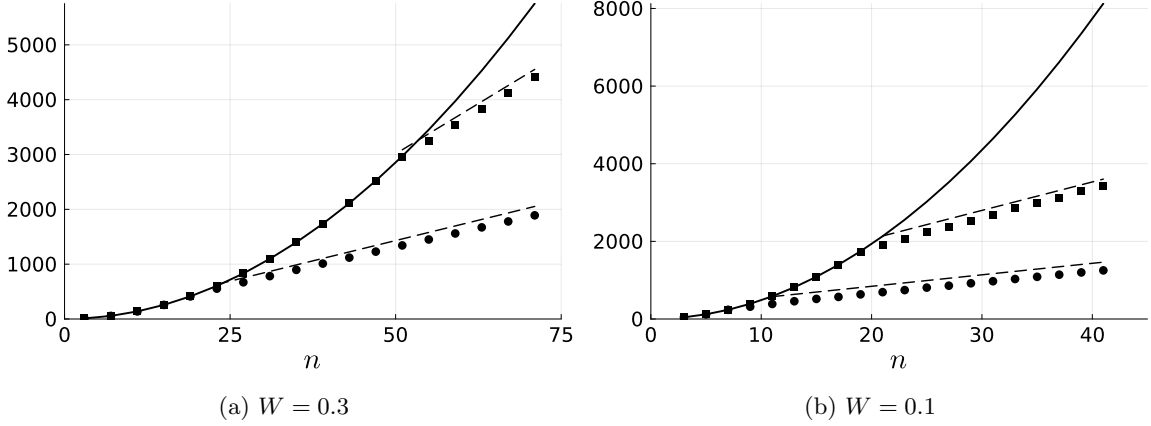


Figure 8: The maximum of the inverse (numerical) Christoffel function for the one-dimensional Fourier extension frame (64) as a function of  $n$ . Full line:  $\|k_n\|_\infty$ , circles:  $\|k_n^\epsilon\|_\infty$  for single precision  $\epsilon = 10 \epsilon_{\text{mach}}^{\text{sp}} \approx 10^{-6}$ , and squares:  $\|k_n^\epsilon\|_\infty$  for double precision  $\epsilon = 10 \epsilon_{\text{mach}}^{\text{dp}} \approx 2 \times 10^{-15}$ . The linear behaviour of  $k_n^\epsilon$  versus the quadratic behaviour of  $k_n$  implies a difference between log-linear and quadratic sampling rates for least squares fitting with uniformly random samples. The dashed lines mark  $5 \log_{10}(1/\epsilon) + C$ , for varying constant  $C$ . They empirically match the behaviour of  $k_n^\epsilon$ .

It remains to examine how the basis functions  $u_i$  behave. As mentioned before, these functions are linked to the discrete prolate spheroidal wave functions. In Appendix D, we summarize known asymptotic results due to Slepian, which indicate that  $\|u_i\|_\infty = \mathcal{O}(\sqrt{n})$  as  $n \rightarrow \infty$  for all  $i$ , such that

$$\|k_n^\epsilon\|_\infty = \mathcal{O}(n \log(n)).$$

This behaviour is verified numerically in Figure 8, which confirms that  $\|k_n\|_\infty = \mathcal{O}(n^2)$ , while  $\|k_n^\epsilon\|_\infty$  appears to grow linearly in  $n$ . This difference translates in the need for log-linear or quadratic oversampling when computing a least squares approximation with or without regularization, respectively, using uniformly random samples.

As an example, we approximate  $f = 1/(1-0.32x)$  on  $[-W, W]$  with  $W = 0.3$  in the Fourier extension frame defined by (64) using uniformly random samples. The approximation is computed using a truncated singular value decomposition (TSVD) solver with threshold  $\epsilon = 10 \epsilon_{\text{mach}}^{\text{dp}} \approx 2 \times 10^{-15}$ , where  $\epsilon_{\text{mach}}^{\text{dp}}$  denotes the working precision associated with IEEE double precision floating point numbers. Figure 9 shows the  $L^2$ -error and demonstrates that linear oversampling suffices for convergence down to machine precision. In contrast, if we were to analyse this problem without taking regularization into account, we would conclude from Theorem 13 that quadratic oversampling is needed.

The approximation seems to converge root-exponentially. For a more detailed analysis of the convergence behaviour, we refer to [9]. Note that convergence is exponential without regularization, see e.g. [36] and the example in section 3, but demands quadratic oversampling. Hence, we get root-exponential convergence as a function of the number of sample points  $m$  with and without regularization. This is an example of a setting where the negative effects of regularization, i.e., reduced accuracy, are balanced by the positive effects, i.e., reduced need for data.

As discussed for the Legendre + weighted Legendre basis in section 6.1.2, it is often preferred to use structured point sets, as they allow for the design of efficient least squares solvers such as the AZ algorithm for frame approximations [22, 31]. However, the analysis of deterministic sample sets is significantly more involved than that of random samples. An extensive analysis of equispaced sample points for polynomial extension frames is presented in [10], which arrives at a very similar conclusion.

**Remark 6.** *What happens if we want to compute an approximation that converges root-exponentially all the way down to zero? In this case, we would need to vary the precision and the regularization parameter with  $n$ :  $\epsilon \sim \epsilon_{\text{mach}} = \exp(-C\sqrt{n})$  for some  $C > 0$ . Following Theorem 14, linear oversampling does not suffice in this case. Specifically, the required linear oversampling factor scales with  $\log(1/\epsilon)$ .*

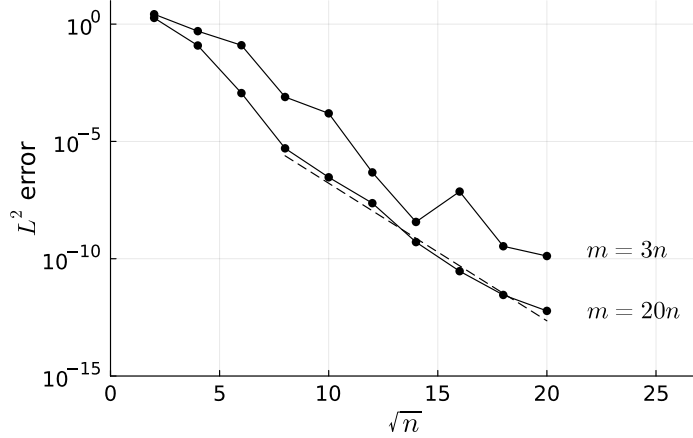


Figure 9: Error of the TSVD approximation of  $f = 1/(1 - 0.32x)$  in the Fourier extension frame defined by (64) for  $W = 0.3$ , using  $m$  uniformly random samples and a truncation threshold  $\epsilon = 10 \epsilon_{\text{mach}}^{\text{dp}} \approx 2 \times 10^{-15}$ . The figure illustrates that linear oversampling suffices for convergence down to machine precision. In contrast, an analysis that ignores the effects of regularization would suggest a need for quadratic oversampling. The approximation appears to converge root-exponentially, while convergence without regularization is exponential but demands quadratic oversampling. Thus, root-exponential convergence as a function of the number of sample points  $m$  occurs both with and without regularization. This is an example of a setting where the negative effects of regularization, i.e., reduced accuracy, are balanced by the positive effects, i.e., reduced need for data.

## A Accuracy of backward stable algorithms

*Proof of Theorem 5.* For any linear operator  $\Delta\mathcal{T}_n$  mapping from  $\mathbb{C}^{n'}$  to  $H$  and any  $\Delta f \in H$ , we have that

$$\|f - \mathcal{T}_n \hat{\mathbf{c}}\|_H \leq \|(f + \Delta f) - (\mathcal{T}_n + \Delta\mathcal{T}_n) \hat{\mathbf{c}}\|_H + \|\Delta f\|_H + \|\Delta\mathcal{T}_n \hat{\mathbf{c}}\|_H.$$

Since  $\hat{\mathbf{c}}$  is computed by a backward stable algorithm with stability constant  $C$ , there exist  $\hat{\Delta}\mathcal{T}_n$  and  $\hat{\Delta}f$  satisfying  $\|\hat{\Delta}\mathcal{T}_n\|_{2,H} \leq C \epsilon_{\text{mach}} \|\mathcal{T}_n\|_{2,H}$  and  $\|\hat{\Delta}f\|_H \leq C \epsilon_{\text{mach}} \|f\|_H$  such that

$$\hat{\mathbf{c}} \in \arg \min_{\mathbf{x} \in \mathbb{C}^{n'}} \|(f + \hat{\Delta}f) - (\mathcal{T}_n + \hat{\Delta}\mathcal{T}_n) \mathbf{x}\|_H.$$

Hence, for all  $\mathbf{x} \in \mathbb{C}^{n'}$  it holds that

$$\begin{aligned} \|f - \mathcal{T}_n \hat{\mathbf{c}}\|_H &\leq \|(f + \hat{\Delta}f) - (\mathcal{T}_n + \hat{\Delta}\mathcal{T}_n) \hat{\mathbf{c}}\|_H + \|\hat{\Delta}f\|_H + \|\hat{\Delta}\mathcal{T}_n \hat{\mathbf{c}}\|_H, \\ &\leq \|(f + \hat{\Delta}f) - (\mathcal{T}_n + \hat{\Delta}\mathcal{T}_n) \mathbf{x}\|_H + \|\hat{\Delta}f\|_H + \|\hat{\Delta}\mathcal{T}_n \hat{\mathbf{c}}\|_H, \\ &\leq \|f - \mathcal{T}_n \mathbf{x}\|_H + 2\|\hat{\Delta}f\|_H + \|\hat{\Delta}\mathcal{T}_n \hat{\mathbf{c}}\|_H + \|\hat{\Delta}\mathcal{T}_n \mathbf{x}\|_H. \end{aligned}$$

The final bound follows from  $\|\hat{\Delta}\mathcal{T}_n\|_{2,H} \leq C \epsilon_{\text{mach}} \|\mathcal{T}_n\|_{2,H}$  and  $\|\hat{\Delta}f\|_H \leq C \epsilon_{\text{mach}} \|f\|_H$ .

For the second result, note that

$$\|\hat{\mathbf{c}}\|_2 = \|(\mathcal{T}_n + \hat{\Delta}\mathcal{T}_n)^\dagger (f + \hat{\Delta}f)\|_2 \leq \frac{\|f + \hat{\Delta}f\|_H}{\sigma_{\min}(\mathcal{T}_n + \hat{\Delta}\mathcal{T}_n)},$$

where  $\sigma_{\min}$  denotes the smallest singular value. Using (19), we obtain  $\sigma_{\min}(\mathcal{T}_n + \hat{\Delta}\mathcal{T}_n) \geq \sigma_{\min}(\mathcal{T}_n) - \|\hat{\Delta}\mathcal{T}_n\|_{2,H} = \sqrt{A_n} - C \epsilon_{\text{mach}} \sqrt{B_n} > 0$ , such that

$$\|\hat{\mathbf{c}}\|_2 \leq \frac{\|f + \hat{\Delta}f\|_H}{\sqrt{A_n} - C \epsilon_{\text{mach}} \sqrt{B_n}}.$$

Furthermore, we have that  $\mathcal{P}_n f \in V_n$  and, hence, there exist coefficients  $\mathbf{c} \in \mathbb{C}^{n'}$  such that  $\mathcal{P}_n f = \mathcal{T}_n \mathbf{c}$  with  $\|\mathbf{c}\|_2 \leq \|\mathcal{P}_n f\|_H / \sqrt{A_n}$  (20). The final result follows from choosing  $\mathbf{x} = \mathbf{c}$ , i.e.,

$$\begin{aligned} \|f - \mathcal{T}_n \hat{\mathbf{c}}\|_H &\leq \|f - \mathcal{T}_n \mathbf{c}\|_H + C \epsilon_{\text{mach}} \left( \sqrt{B_n} (\|\hat{\mathbf{c}}\|_2 + \|\mathbf{c}\|_2) + 2\|f\|_H \right) \\ &\leq \|f - \mathcal{P}_n f\|_H + C \epsilon_{\text{mach}} \left( \sqrt{B_n} \left( \frac{\|f + \hat{\Delta} f\|_H}{\sqrt{A_n} - C \epsilon_{\text{mach}} \sqrt{B_n}} + \frac{\|\mathcal{P}_n f\|_H}{\sqrt{A_n}} \right) + 2\|f\|_H \right) \\ &\leq \|f - \mathcal{P}_n f\|_H + C \epsilon_{\text{mach}} \left( \frac{(1 + C \epsilon_{\text{mach}}) \sqrt{B_n}}{\sqrt{A_n} - C \epsilon_{\text{mach}} \sqrt{B_n}} + \sqrt{\frac{B_n}{A_n}} + 2 \right) \|f\|_H. \end{aligned}$$

□

*Proof of Theorem 6.* For any linear operator  $\Delta \mathcal{T}_n$  mapping from  $\mathbb{C}^{n'}$  to  $H$  and any  $\Delta f \in H$ , we have that

$$\|f - \mathcal{T}_n \hat{\mathbf{c}}\|_H \leq \|(f + \Delta f) - (\mathcal{T}_n + \Delta \mathcal{T}_n) \hat{\mathbf{c}}\|_H + \|\Delta f\|_H + \|\Delta \mathcal{T}_n \hat{\mathbf{c}}\|_H.$$

Since  $\hat{\mathbf{c}}$  is computed by a backward stable algorithm with stability constant  $C$ , there exist  $\hat{\Delta} \mathcal{T}_n$  and  $\hat{\Delta} f$  satisfying  $\|\hat{\Delta} \mathcal{T}_n\|_{2,H} \leq C \epsilon_{\text{mach}} \|\mathcal{T}_n\|_{2,H}$  and  $\|\hat{\Delta} f\|_H \leq C \epsilon_{\text{mach}} \|f\|_H$  such that

$$\hat{\mathbf{c}} = \arg \min_{\mathbf{x} \in \mathbb{C}^{i_n}} \|(f + \hat{\Delta} f) - (\mathcal{T}_n + \hat{\Delta} \mathcal{T}_n) \mathbf{x}\|_H^2 + \epsilon^2 \|\mathbf{x}\|_2^2.$$

Therefore, for all  $\mathbf{x} \in \mathbb{C}^{n'}$ ,

$$\begin{aligned} \|(f + \hat{\Delta} f) - (\mathcal{T}_n + \hat{\Delta} \mathcal{T}_n) \hat{\mathbf{c}}\|_H^2 + \epsilon^2 \|\hat{\mathbf{c}}\|_2^2 &\leq \|(f + \hat{\Delta} f) - (\mathcal{T}_n + \hat{\Delta} \mathcal{T}_n) \mathbf{x}\|_H^2 + \epsilon^2 \|\mathbf{x}\|_2^2 \\ \Rightarrow \|(f + \hat{\Delta} f) - (\mathcal{T}_n + \hat{\Delta} \mathcal{T}_n) \hat{\mathbf{c}}\|_H + \epsilon \|\hat{\mathbf{c}}\|_2 &\leq \sqrt{2} \left( \|(f + \hat{\Delta} f) - (\mathcal{T}_n + \hat{\Delta} \mathcal{T}_n) \mathbf{x}\|_H + \epsilon \|\mathbf{x}\|_2 \right). \end{aligned}$$

Hence, it holds that

$$\begin{aligned} \|f - \mathcal{T}_n \hat{\mathbf{c}}\|_H &\leq \|(f + \hat{\Delta} f) - (\mathcal{T}_n + \hat{\Delta} \mathcal{T}_n) \hat{\mathbf{c}}\|_H + \|\hat{\Delta} f\|_H + \|\hat{\Delta} \mathcal{T}_n \hat{\mathbf{c}}\|_H, \\ &\leq \|(f + \hat{\Delta} f) - (\mathcal{T}_n + \hat{\Delta} \mathcal{T}_n) \hat{\mathbf{c}}\|_H + C \epsilon_{\text{mach}} \|f\|_H + \epsilon \|\hat{\mathbf{c}}\|_2, \\ &\leq \sqrt{2} \left( \|(f + \hat{\Delta} f) - (\mathcal{T}_n + \hat{\Delta} \mathcal{T}_n) \mathbf{x}\|_H + \epsilon \|\mathbf{x}\|_2 \right) + C \epsilon_{\text{mach}} \|f\|_H, \\ &\leq \sqrt{2} \|f - \mathcal{T}_n \mathbf{x}\|_H + (1 + \sqrt{2}) \epsilon \|\mathbf{x}\|_2 + (1 + \sqrt{2}) C \epsilon_{\text{mach}} \|f\|_H, \end{aligned}$$

where in the second step it was used that  $\epsilon \geq C \epsilon_{\text{mach}} \|\mathcal{T}_n\|_{2,H}$ . □

## B Proof of Theorem 10

For completeness, we first prove an equivalent characterization of (48).

**Lemma 4.** For any  $\epsilon > 0$ ,

$$k_n^\epsilon(\mathbf{x}) = \phi(\mathbf{x})(G_n + \epsilon^2 I)^{-1} \phi(\mathbf{x})^*,$$

where  $\phi(\mathbf{x}) = [\phi_1(\mathbf{x}) \ \dots \ \phi_{n'}(\mathbf{x})] \in \mathbb{C}^{1 \times n'}$  and  $G_n$  represents  $\mathcal{T}_n^* \mathcal{T}_n$ .

*Proof.*  $G_n$  is positive semidefinite and, hence, there exists an eigenvalue decomposition of the form  $V \Sigma^2 V^*$ , where  $V \in \mathbb{C}^{n' \times n'}$  is unitary and  $\Sigma \in \mathbb{C}^{n' \times n'}$  is diagonal. Moreover, this implies that the synthesis operator  $\mathcal{T}_n$  associated with  $\Phi_n$  has a singular value decomposition of the form  $\sum_{i=1}^n \sigma_i u_i \mathbf{v}_i^*$  where  $\{u_i\}_{i=1}^n$  is an orthonormal basis for  $V_n$ ,  $\mathbf{v}_i$  are the first  $n$  columns of  $V$  and  $\sigma_i = (\Sigma)_{i,i}$  for  $i = 1 \dots n$ . Therefore, using  $\phi(\mathbf{x}) = \sum_{i=1}^n \sigma_i u_i(\mathbf{x}) \mathbf{v}_i^*$ , we obtain

$$\begin{aligned} \phi(\mathbf{x})(G_n + \epsilon^2 I)^{-1} \phi(\mathbf{x})^* &= \left( \sum_{i=1}^n \sigma_i u_i(\mathbf{x}) \mathbf{v}_i^* \right) V (\Sigma^2 + \epsilon^2 I)^{-1} V^* \left( \sum_{i=1}^n \sigma_i \overline{u_i(\mathbf{x})} \mathbf{v}_i \right) \\ &= \left( \sum_{i=1}^n \sigma_i u_i(\mathbf{x}) \mathbf{v}_i^* V \right) (\Sigma^2 + \epsilon^2 I)^{-1} \left( \sum_{i=1}^n \sigma_i \overline{u_i(\mathbf{x})} V^* \mathbf{v}_i \right) \\ &= [\sigma_1 u_1(\mathbf{x}) \ \dots \ \sigma_n u_n(\mathbf{x})] (\Sigma^2 + \epsilon^2 I)^{-1} [\sigma_1 \overline{u_1(\mathbf{x})} \ \dots \ \sigma_n \overline{u_n(\mathbf{x})}]^\top \\ &= \sum_{i=1}^n \frac{\sigma_i^2}{\sigma_i^2 + \epsilon^2} |u_i(\mathbf{x})|^2, \end{aligned}$$

which equals (48). □

We are now ready to prove Theorem 10.

*Proof of Theorem 10.* Note that

$$\frac{1}{2}(G_n + \epsilon^2 I) \preceq G_{n,m} + \epsilon^2 I \preceq \frac{3}{2}(G_n + \epsilon^2 I) \quad \Rightarrow \quad (35) \text{ with } A_{n,m}^\epsilon = \frac{1}{2}.$$

The inequality on the left is exactly the  $\Delta$ -spectral approximation introduced in [12, eq. (2)] with  $\Delta = 1/2$ . This allows us to reuse the method of proof of [12, Lemma 6]. Analogously, using the eigenvalue decomposition of  $G_n + \epsilon^2 I = V \Sigma^2 V^*$  we find that it suffices to show that

$$\|\Sigma^{-1} V^* G_{n,m} V \Sigma^{-1} - \Sigma^{-1} V^* G_n V \Sigma^{-1}\|_2 \leq 1/2$$

holds with probability  $1 - \gamma$ . Define a rank-one random matrix

$$X(\mathbf{x}) = w(\mathbf{x}) \Sigma^{-1} V^* \phi(\mathbf{x})^* \phi(\mathbf{x}) V \Sigma^{-1},$$

where  $\mathbf{x}$  is distributed according to  $\mu$  and where  $\phi(\mathbf{x})$  is defined as in Lemma 4. Then,  $\Sigma^{-1} V^* G_{n,m} V \Sigma^{-1}$  is equal to the sum of  $m$  i.i.d. copies of this random matrix, i.e.,

$$\Sigma^{-1} V^* G_{n,m} V \Sigma^{-1} = \frac{1}{m} \sum_{j=1}^m X_j.$$

Since  $\mathbb{E}(X_j) = \Sigma^{-1} V^* G_n V \Sigma^{-1}$ , we can use the matrix concentration result [12, Lemma 27]. Using Lemma 4, we bound

$$\|X_j\|_2 = w(\mathbf{x}_j) \phi(\mathbf{x}_j) (G_n + \epsilon^2 I)^{-1} \phi(\mathbf{x}_j)^* = w(\mathbf{x}_j) k_n^\epsilon(\mathbf{x}_j) \leq K_{w,n}^\epsilon,$$

and

$$\mathbb{E}(X_j^2) = \mathbb{E}(w(\mathbf{x}_j) k_n^\epsilon(\mathbf{x}_j) X_j) \preceq K_{w,n}^\epsilon \Sigma^{-1} V^* G_n V \Sigma^{-1} = K_{w,n}^\epsilon (I - \epsilon^2 \Sigma^{-2}),$$

where  $K_{w,n}^\epsilon := \max_{\mathbf{x} \in X} |w(\mathbf{x}) k_n^\epsilon(\mathbf{x})|$  and  $I \in \mathbb{R}^{n \times n}$  is the identity matrix. Defining

$$E := K_{w,n}^\epsilon (I - \epsilon^2 \Sigma^{-2}) = K_{w,n}^\epsilon \text{diag}(\sigma_1^2 / (\sigma_1^2 + \epsilon^2), \dots, \sigma_n^2 / (\sigma_n^2 + \epsilon^2)),$$

where  $\sigma_i$  is the  $i$ -th singular value of  $\mathcal{T}_n$ , this results in

$$\begin{aligned} \Pr \left( \left\| \frac{1}{m} \sum_{j=1}^m X_j - \Sigma^{-1} V^* G_n V \Sigma^{-1} \right\|_2 \geq 1/2 \right) &\leq \frac{8 \text{Tr}(E)}{\|E\|_2} \exp \left( \frac{-m/8}{\|E\|_2 + K_{w,n}^\epsilon/3} \right) \\ &\leq 16n^\epsilon \exp \left( \frac{-3}{32} \frac{m}{K_{w,n}^\epsilon} \right) \leq \gamma \end{aligned}$$

where in the second step we used the assumption  $\sigma_1^2 = \|G\|_2 \geq \epsilon^2$ . □

## C Proof of Theorem 11

*Proof of Theorem 11.* Equation (57) follows immediately from splitting the summation that defines  $n^\epsilon$  as

$$n^\epsilon = \sum_{i=1}^n \frac{\sigma_i^2}{\sigma_i^2 + \epsilon^2} = \sum_{i=1}^{i_2} \frac{\sigma_i^2}{\sigma_i^2 + \epsilon^2} + \sum_{i=i_2+1}^n \frac{\sigma_i^2}{\sigma_i^2 + \epsilon^2} \leq \sum_{i=1}^{i_2} 1 + \sum_{i=i_2+1}^n \frac{\sigma_i^2}{\epsilon^2} = i_2 + S_{\text{tail}}.$$

For (58), consider

$$k_n^{\text{trunc}}(\mathbf{x}) = \sum_{i=1}^{i_2} |u_i(\mathbf{x})|^2 \leq 2 \sum_{i=1}^{i_2} \frac{\sigma_i^2}{\sigma_i^2 + \epsilon^2} |u_i(\mathbf{x})|^2 \leq 2 \sum_{i=1}^n \frac{\sigma_i^2}{\sigma_i^2 + \epsilon^2} |u_i(\mathbf{x})|^2 = 2k_n^\epsilon(\mathbf{x})$$

and

$$k_n^\epsilon(\mathbf{x}) = \sum_{i=1}^n \frac{\sigma_i^2}{\sigma_i^2 + \epsilon^2} |u_i(\mathbf{x})|^2 \leq \sum_{i=1}^{i_2} |u_i(\mathbf{x})|^2 + \sum_{i=i_2+1}^n \frac{\sigma_i^2}{\epsilon^2} |u_i(\mathbf{x})|^2 \leq k_n^{\text{trunc}}(\mathbf{x}) + S_{\text{tail}} \max_{i_2 < i \leq n} |u_i(\mathbf{x})|^2.$$

In order to obtain (59), we split the above as

$$\begin{aligned} \|k_n^\epsilon\|_\infty &\leq \sup_{\mathbf{x} \in X} \left( \sum_{i=1}^{i_1} |u_i(\mathbf{x})|^2 + \sum_{i=i_1+1}^{i_2} |u_i(\mathbf{x})|^2 + S_{\text{tail}} \max_{i_2 < i \leq n} |u_i(\mathbf{x})|^2 \right) \\ &\leq \sup_{\mathbf{x} \in X} \sum_{i=1}^{i_1} |u_i(\mathbf{x})|^2 + ((i_2 - i_1) + S_{\text{tail}}) \max_{i_1 < i \leq n} \|u_i\|_\infty^2. \end{aligned}$$

The first term can be bounded using the singular value decomposition of  $\mathcal{T}_n$

$$\sum_{i=1}^{i_1} |u_i(\mathbf{x})|^2 = \|\phi(\mathbf{x})VD^{-1}\|_2^2 \leq \|\phi(\mathbf{x})\|_2^2 \|V\|_2^2 \|D^{-1}\|_2^2 = \frac{\|\phi(\mathbf{x})\|_2^2}{\sigma_{i_1}^2} \leq \frac{\|\phi(\mathbf{x})\|_2^2}{1 - \epsilon^2},$$

where  $\phi(\mathbf{x}) = [\phi_{1,n}(\mathbf{x}) \ \dots \ \phi_{n,n}(\mathbf{x})]$ ,  $V \in \mathbb{C}^{n \times i_1}$  is a matrix with orthogonal columns and  $D \in \mathbb{C}^{i_1 \times i_1}$  is a diagonal matrix with  $(D)_{(i,i)} = \sigma_i$ . The final result follows from

$$\sup_{\mathbf{x} \in X} \frac{\|\phi(\mathbf{x})\|_2^2}{1 - \epsilon^2} \leq \frac{1}{1 - \epsilon^2} \sup_{\mathbf{x} \in X} \sum_{i=1}^n |\phi_{i,n}(\mathbf{x})|^2 \leq \frac{1}{1 - \epsilon^2} \sum_{i=1}^n \|\phi_{i,n}\|_\infty^2 \leq \frac{n}{1 - \epsilon^2}.$$

□

## D Asymptotics of DPSWFs

In this section, we aim to motivate that the maxima  $\|u_i\|_\infty$  associated to the one-dimensional Fourier extension frame (64) are  $\mathcal{O}(\sqrt{n})$  as  $n \rightarrow \infty$ . In order to do so, observe that

$$\|u_i\|_\infty = \|U_{i-1}(n, W)\|_\infty / \sqrt{\lambda_{i-1}(n, W)}, \quad (70)$$

where  $U_k(n, W)$  and  $\lambda_k(n, W)$  are the discrete prolate spheroidal wave functions (DPSWFs) and the associated eigenvalues analysed by Slepian in [50]. We recall and examine their asymptotic behaviour for the different regimes identified in [50, section 2.4-2.5]. Numerical evidence confirms that (70) is bounded by  $\mathcal{O}(\sqrt{n})$ , as is the case for the prolate spheroidal wave functions [16, Prop. 3.1], the continuous analogues of the DPSWFs.

Given the asymptotic expansions outlined in [50, section 2.4-2.5], we can derive that as  $n \rightarrow \infty$ :

- for  $i \leq 2nW + 1$ ,

$$\|u_i\|_\infty = \mathcal{O}(\sqrt{n}), \quad (71)$$

- for  $i = \lfloor 2nW + (b/\pi) \log(n) \rfloor + 1$  with fixed  $b > 0$ ,

$$\|u_i\|_\infty \sim r(E\beta) \sqrt{\beta} \exp(\pi E\beta/4) \sqrt{\frac{3\pi(1 + \exp(\pi b))}{\beta(1 + \exp(\pi E\beta)) \ln(n)}} \sqrt{n}, \quad (72)$$

where  $r$ ,  $E$  and  $\beta$  are defined by [50, eq. (52)-(54)],

- for  $i = \lfloor 2nW(1 + \epsilon) \rfloor + 1$  with fixed  $0 < \epsilon < 1/2W - 1$ ,

$$\|u_i\|_\infty \sim L_2^{-1/2} \pi (1 - \cos(2\pi W))^2)^{-1/4} \sqrt{n}, \quad (73)$$

where  $L_2$  is defined by [50, eq. (47)] with  $A = -\cos(2\pi W)$  and  $k = n - (i - 1)$ ,

- for  $i = n - l$  with fixed  $0 \leq l$ ,

$$\|u_i\|_\infty \sim \sqrt{\pi} \left( \frac{2}{1 - \cos(2\pi W)} \right)^{1/4} \sqrt{n}. \quad (74)$$

The result for  $i \leq 2nW + 1$  follows from considering

$$\begin{aligned} \|u_i\|_{\infty, [-W, W]} &\leq \|u_i\|_{\infty, [-1/2, 1/2]} \\ &= \|U_{i-1}(n, W)\|_{\infty, [-1/2, 1/2]} / \sqrt{\lambda_{i-1}(n, W)} \\ &\leq \sqrt{n} / \sqrt{\lambda_{i-1}(n, W)}, \end{aligned}$$

where we used the Nikolskii inequality [43, Theorem 1] with  $\|U_{i-1}(n, W)\|_{\infty, [-1/2, 1/2]} = 1$ . Furthermore,

$$1/\sqrt{\lambda_{i-1}(n, W)} \leq 1/\sqrt{\lambda_{\lfloor 2nW \rfloor}(n, W)} \sim \sqrt{2}$$

using [50, eq. (60)]. Hence, we get  $\|u_i\|_{\infty, [-W, W]} = \mathcal{O}(\sqrt{n})$ , where the proportionality factor is at most approximately  $\sqrt{2}$ .

For the case of  $i \geq 2nW + 1$ , it follows from [47, Corollary 2] and the fact that the DPSWFs are even or odd that

$$\|u_i\|_\infty = \frac{\|U_{i-1}(n, W)\|_\infty}{\sqrt{\lambda_{i-1}(n, W)}} = \frac{|U_{i-1}(n, W; \omega = 2\pi W)|}{\sqrt{\lambda_{i-1}(n, W)}}.$$

Hence, the maximum is achieved at the boundary. Furthermore, by combining [50, eq. (50) and (60)] for  $U_k(n, W)$  and  $\lambda_k(n, W)$  for  $k = i - 1 = \lfloor 2nW + (b/\pi) \log(n) \rfloor$  with fixed  $b$ , one obtains

$$\frac{|U_k(n, W; \omega = 2\pi W)|}{\sqrt{\lambda_k(n, W)}} \sim r(E\beta) \sqrt{\beta} \exp(\pi E\beta/4) \sqrt{\frac{3\pi(1 + \exp(\pi b))}{\beta(1 + \exp(\pi E\beta)) \ln(n)}} \sqrt{n}$$

Similarly, for  $k = i - 1 = \lfloor 2nW(1 + \epsilon) \rfloor$  with fixed  $0 < \epsilon < 1/2W - 1$  we derive from [50, eq. (42), (56), (57) and (63)] that

$$\frac{|U_k(n, W; \omega = 2\pi W)|}{\sqrt{\lambda_k(n, W)}} \sim L_2^{-1/2} \pi (1 - \cos(2\pi W))^2)^{-1/4} \sqrt{n},$$

while for  $k = i - 1 = n - l$  with fixed  $l \geq 1$  we derive from [50, eq. (13), (38) and (58)] that

$$\frac{|U_k(n, W; \omega = 2\pi W)|}{\sqrt{\lambda_k(n, W)}} \sim \sqrt{\pi} \left( \frac{2}{1 - \cos(2\pi W)} \right)^{1/4} \sqrt{n}.$$

## Acknowledgements

We greatly appreciate the fruitful discussions and helpful suggestions provided by Ben Adcock, Felix Bartel, Nick Dewaele, Karlheinz Gröchenig, Christopher Musco, Thijs Steel, Alex Townsend, Nick Trefethen, and Raf Vandebril.

## Funding

The first author is a Ph.D fellow of the Research Foundation Flanders (FWO), funded by grant 11P2T24N.

## References

- [1] B. Adcock. Optimal sampling for least-squares approximation. *arXiv preprint arXiv:2409.02342*, 2024.

- [2] B. Adcock, S. Brugiapaglia, and C. G. Webster. *Sparse Polynomial Approximation of High-Dimensional Functions*. SIAM, Philadelphia, PA, 2022.
- [3] B. Adcock, J. M. Cardenas, and N. Dexter. CAS4DL: Christoffel adaptive sampling for function approximation via deep learning. *Sampl. Theory Signal Process. Data Anal.*, 20(2):21, 2022.
- [4] B. Adcock and A. C. Hansen. A generalized sampling theorem for stable reconstructions in arbitrary bases. *J. Fourier Anal. Appl.*, 18:685–716, 2012.
- [5] B. Adcock, A. C. Hansen, and C. Poon. Beyond consistent reconstructions: Optimality and sharp bounds for generalized sampling, and application to the uniform resampling problem. *SIAM J. Math. Anal.*, 45(5):3132–3167, 2013.
- [6] B. Adcock and D. Huybrechs. Frames and numerical approximation. *SIAM Rev.*, 61(3):443–473, 2019.
- [7] B. Adcock and D. Huybrechs. Approximating smooth, multivariate functions on irregular domains. In *Forum Math. Sigma*, volume 8, page e26, 2020.
- [8] B. Adcock and D. Huybrechs. Frames and numerical approximation II: Generalized sampling. *J. Fourier Anal. Appl.*, 26(6):87, 2020.
- [9] B. Adcock, D. Huybrechs, and J. Martín-Vaquero. On the numerical stability of Fourier extensions. *Found. Comput. Math.*, 14(4):635–687, 2014.
- [10] B. Adcock and A. Shadrin. Fast and stable approximation of analytic functions from equispaced samples via polynomial frames. *Constr. Approx.*, 57(2):257–294, 2023.
- [11] A. Alaoui and M. W. Mahoney. Fast randomized kernel ridge regression with statistical guarantees. *Adv. Neural Inf. Process. Syst.*, 28:775–783, 2015.
- [12] H. Avron, M. Kapralov, C. Musco, C. Musco, A. Velingker, and A. Zandieh. Random Fourier features for kernel ridge regression: Approximation bounds and statistical guarantees. In *Int. Conf. Mach. Learn. ICML*, pages 253–262. PMLR, 2017.
- [13] H. Avron, M. Kapralov, C. Musco, C. Musco, A. Velingker, and A. Zandieh. A universal sampling method for reconstructing signals with simple Fourier transforms. In *Proc. 51st Annu. ACM SIGACT Symp. Theory Comput.*, STOC 2019, pages 1051–1063. Association for Computing Machinery, 2019.
- [14] P. Berger, K. Gröchenig, and G. Matz. Sampling and reconstruction in distinct subspaces using oblique projections. *J. Fourier Anal. Appl.*, 25(3):1080–1112, 2019.
- [15] R. Bhatia. *Notes on Functional Analysis*. Hindustan Book Agency, New Delhi, 2009.
- [16] A. Bonami, G. Kerkyacharian, and P. Petrushev. Gaussian bounds for the heat kernel associated to prolate spheroidal wave functions with applications. *Constr. Approx.*, 57(2):351–403, 2023.
- [17] J. P. Boyd. *Chebyshev and Fourier Spectral Methods*. Dover Publications, Mineola, NY, 2nd edition, 2001.
- [18] P. D. Brubeck, Y. Nakatsukasa, and L. N. Trefethen. Vandermonde with Arnoldi. *SIAM Rev.*, 63(2):405–415, 2021.
- [19] O. Christensen et al. *An Introduction to Frames and Riesz Bases*. Birkhäuser, Basel, 2003.
- [20] A. Cohen, M. A. Davenport, and D. Leviatan. On the stability and accuracy of least squares approximations. *Found. Comput. Math.*, 13:819–834, 2013.
- [21] A. Cohen and G. Migliorati. Optimal weighted least-squares methods. *SMAI J. Comput. Math.*, 3:181–203, 2017.
- [22] V. Coppé, D. Huybrechs, R. Matthysen, and M. Webb. The AZ algorithm for least squares systems with a known incomplete generalized inverse. *SIAM J. Matrix Anal. Appl.*, 41(3):1237–1259, 2020.

- [23] I. Daubechies. *Ten Lectures on Wavelets*. SIAM, Philadelphia, PA, 1992.
- [24] E. B. Davies and M. Plum. Spectral pollution. *IMA J. Numer. Anal.*, 24(3):417–438, 2004.
- [25] M. Dolbeault and A. Cohen. Optimal sampling and Christoffel functions on general domains. *Constr. Approx.*, 56(1):121–163, 2022.
- [26] T. A. Driscoll, N. Hale, and L. N. Trefethen. *Chebfun Guide*. Pafnuty Publications, Oxford, 2014.
- [27] Z. Drmac. On principal angles between subspaces of euclidean space. *SIAM J. Matrix Anal. Appl.*, 22(1):173–194, 2000.
- [28] W. Gautschi. *Orthogonal Polynomials: Computation and Approximation*. Oxford University Press, Oxford, 2004.
- [29] G. Golub. *Rosetak Document 4: Rank Degeneracies and Least Square Problems*. NBER Working Paper Series No. W0165. National Bureau of Economic Research, Cambridge, Mass, 1977.
- [30] K. Gröchenig. Sampling, Marcinkiewicz–Zygmund inequalities, approximation, and quadrature rules. *J. Approx. Theory*, 257:105455, 2020.
- [31] A. Herremans and D. Huybrechs. Efficient function approximation in enriched approximation spaces. *IMA J. Numer. Anal.*, page drae017, 2024.
- [32] A. Herremans and D. Huybrechs. SamplingWithNumericalRedundancy. <https://github.com/aherremans/SamplingWithNumericalRedundancy>, 2025.
- [33] A. Herremans, D. Huybrechs, and L. N. Trefethen. Resolution of singularities by rational functions. *SIAM J. Numer. Anal.*, 61(6):2580–2600, 2023.
- [34] N. J. Higham. The accuracy of solutions to triangular systems. *SIAM J. Numer. Anal.*, 26(5):1252–1265, 1989.
- [35] N. J. Higham. *Accuracy and Stability of Numerical Algorithms*. SIAM, Philadelphia, PA, 2nd edition, 2002.
- [36] D. Huybrechs. On the Fourier extension of nonperiodic functions. *SIAM J. Numer. Anal.*, 47(6):4326–4355, 2010.
- [37] D. Huybrechs and A.-E. Olteanu. An oversampled collocation approach of the wave based method for Helmholtz problems. *Wave Motion*, 87:92–105, 2019.
- [38] S. Karnik, J. Romberg, and M. A. Davenport. Improved bounds for the eigenvalues of prolate spheroidal wave functions and discrete prolate spheroidal sequences. *Appl. Comput. Harmon. Anal.*, 55:97–128, 2021.
- [39] H. J. Landau and H. O. Pollak. Prolate spheroidal wave functions, Fourier analysis and uncertainty—III: The dimension of the space of essentially time- and band-limited signals. *Bell Syst. Tech. J.*, 41(4):1295–1336, 1962.
- [40] R. Matthysen and D. Huybrechs. Function approximation on arbitrary domains using Fourier extension frames. *SIAM J. Numer. Anal.*, 56(3):1360–1385, 2018.
- [41] R. A. Meyer, C. Musco, C. Musco, D. P. Woodruff, and S. Zhou. Near-linear sample complexity for  $L_p$  polynomial regression. In *Proc. 2023 Annu. ACM-SIAM Symp. Discrete Algorithms SODA*, pages 3959–4025. SIAM, 2023.
- [42] G. Migliorati. Multivariate approximation of functions on irregular domains by weighted least-squares methods. *IMA J. Numer. Anal.*, 41(2):1293–1317, 2021.
- [43] R. J. Nessel and G. Wilmes. Nikolskii-type inequalities for trigonometric polynomials and entire functions of exponential type. *J. Aust. Math. Soc.*, 25(1):7–18, 1978.

- [44] P. Nevai. Géza Freud, orthogonal polynomials and Christoffel functions. A case study. *J. Approx. Theory*, 48(1):3–167, 1986.
- [45] I. Papadopoulos, T. S. Gutleb, J. A. Carrillo, and S. Olver. A frame approach for equations involving the fractional laplacian. *arXiv preprint arXiv:2311.12451*, 2023.
- [46] C. Piret. A radial basis function based frames strategy for bypassing the Runge phenomenon. *SIAM J. Sci. Comput.*, 38(4):A2262–A2282, 2016.
- [47] K. A. Said and A. A. Beex. Non-asymptotic bounds for discrete prolate spheroidal wave functions analogous with prolate spheroidal wave function bounds. *Appl. Comput. Harmon. Anal.*, 63:20–47, 2023.
- [48] P. F. Shustin and H. Avron. Semi-infinite linear regression and its applications. *SIAM J. Matrix Anal. Appl.*, 43(1):479–511, 2022.
- [49] R. D. Skeel. Scaling for numerical stability in Gaussian elimination. *J. ACM*, 26(3):494–526, 1979.
- [50] D. Slepian. Prolate spheroidal wave functions, Fourier analysis, and uncertainty—V: The discrete case. *Bell Syst. Tech. J.*, 57(5):1371–1430, 1978.
- [51] G. W. Stewart. *Matrix Algorithms: Volume 1: Basic Decompositions*. SIAM, Philadelphia, PA, 1988.
- [52] N. Stylianopoulos. Strong asymptotics for Bergman polynomials over domains with corners and applications. *Constr. Approx.*, 38(1):59–100, 2013.
- [53] N. Stylianopoulos. An Arnoldi Gram-Schmidt process and Hessenberg matrices for orthonormal polynomials. Slides from talk at Banff International Research Station, 2010.
- [54] M. Webb, V. Coppé, and D. Huybrechs. Pointwise and uniform convergence of Fourier extensions. *Constr. Approx.*, 52(1):139–175, 2020.